

# Planck intermediate results. VII. Statistical properties of infrared and radio extragalactic sources from the *Planck* Early Release Compact Source Catalogue at frequencies between 100 and 857 GHz

Planck Collaboration: P. A. R. Ade<sup>84</sup>, N. Aghanim<sup>59</sup>, F. Argüeso<sup>19</sup>, M. Arnaud<sup>73</sup>, M. Ashdown<sup>70,5</sup>, F. Atrio-Barandela<sup>17</sup>, J. Aumont<sup>59</sup>, C. Baccigalupi<sup>83</sup>, A. Balbi<sup>36</sup>, A. J. Banday<sup>88,8</sup>, R. B. Barreiro<sup>67</sup>, E. Battaner<sup>90</sup>, K. Benabed<sup>60,87</sup>, A. Benoît<sup>57</sup>, J.-P. Bernard<sup>8</sup>, M. Bersanelli<sup>33,50</sup>, M. Bethermin<sup>73</sup>, R. Bhatia<sup>6</sup>, A. Bonaldi<sup>69</sup>, J. R. Bond<sup>7</sup>, J. Borrill<sup>12,85</sup>, F. R. Bouchet<sup>60,87</sup>, C. Burigana<sup>49,35</sup>, P. Cabella<sup>37</sup>, J.-F. Cardoso<sup>74,1,60</sup>, A. Catalano<sup>75,72</sup>, L. Cayón<sup>30</sup>, A. Chamballu<sup>55</sup>, R.-R. Chary<sup>56</sup>, X. Chen<sup>56</sup>, L.-Y. Chiang<sup>63</sup>, P. R. Christensen<sup>80,38</sup>, D. L. Clements<sup>55</sup>, S. Colafrancesco<sup>46</sup>, S. Colombi<sup>60,87</sup>, L. P. L. Colombo<sup>22,68</sup>, A. Coulais<sup>72</sup>, B. P. Crill<sup>68,81</sup>, F. Cuttaia<sup>49</sup>, L. Danese<sup>83</sup>, R. J. Davis<sup>69</sup>, P. de Bernardis<sup>32</sup>, G. de Gasperis<sup>36</sup>, G. de Zotti<sup>45,83</sup>, J. Delabrouille<sup>1</sup>, C. Dickinson<sup>69</sup>, J. M. Diego<sup>67</sup>, H. Dole<sup>59,58</sup>, S. Donzelli<sup>50</sup>, O. Doré<sup>68,9</sup>, U. Dörl<sup>78</sup>, M. Douspis<sup>59</sup>, X. Dupac<sup>41</sup>, G. Efstathiou<sup>64</sup>, T. A. Enßlin<sup>78</sup>, H. K. Eriksen<sup>65</sup>, F. Finelli<sup>49</sup>, O. Forni<sup>88,8</sup>, P. Fosalba<sup>61</sup>, M. Frailis<sup>47</sup>, E. Franceschi<sup>49</sup>, S. Galeotta<sup>47</sup>, K. Ganga<sup>1</sup>, M. Giard<sup>188,8</sup>, G. Giardino<sup>42</sup>, Y. Giraud-Héraud<sup>1</sup>, J. González-Nuevo<sup>67,83</sup>, K. M. Górski<sup>68,91</sup>, A. Gregorio<sup>34,47</sup>, A. Gruppuso<sup>49</sup>, F. K. Hansen<sup>65</sup>, D. Harrison<sup>64,70</sup>, S. Henrot-Versillé<sup>71</sup>, C. Hernández-Monteagudo<sup>11,78</sup>, D. Herranz<sup>67</sup>, S. R. Hildebrandt<sup>9</sup>, E. Hivon<sup>60,87</sup>, M. Hobson<sup>5</sup>, W. A. Holmes<sup>68</sup>, T. R. Jaffe<sup>88,8</sup>, A. H. Jaffe<sup>55</sup>, T. Jagemann<sup>41</sup>, W. C. Jones<sup>25</sup>, M. Juvela<sup>24</sup>, E. Keihänen<sup>24</sup>, T. S. Kisner<sup>77</sup>, R. Kneissl<sup>40,6</sup>, J. Knoche<sup>78</sup>, L. Knox<sup>27</sup>, M. Kunz<sup>16,59</sup>, N. Kurinsky<sup>23</sup>, H. Kurki-Suonio<sup>24,44</sup>, G. Lagache<sup>59</sup>, A. Lähteenmäki<sup>2,44</sup>, J.-M. Lamarre<sup>72</sup>, A. Lasenby<sup>5,70</sup>, C. R. Lawrence<sup>68</sup>, R. Leonardi<sup>41</sup>, P. B. Lilje<sup>65,10</sup>, M. López-Caniego<sup>67</sup>, J. F. Macías-Pérez<sup>75</sup>, D. Maino<sup>33,50</sup>, N. Mandolesi<sup>49,4</sup>, M. Maris<sup>47</sup>, D. J. Marshall<sup>88,8</sup>, E. Martínez-González<sup>67</sup>, S. Masi<sup>32</sup>, M. Massardi<sup>48</sup>, S. Matarrese<sup>31</sup>, P. Mazzotta<sup>36</sup>, A. Melchiorri<sup>32,51</sup>, L. Mendes<sup>41</sup>, A. Mennella<sup>33,50</sup>, S. Mitra<sup>54,68</sup>, M.-A. Miville-Deschênes<sup>59,7</sup>, A. Moneti<sup>60</sup>, L. Montier<sup>88,8</sup>, G. Morgante<sup>49</sup>, D. Mortlock<sup>55</sup>, D. Munshi<sup>84</sup>, J. A. Murphy<sup>79</sup>, P. Naselsky<sup>80,38</sup>, F. Nati<sup>32</sup>, P. Natoli<sup>35,3,49</sup>, H. U. Nørgaard-Nielsen<sup>15</sup>, F. Noviello<sup>69</sup>, S. Osborne<sup>86</sup>, F. Pajot<sup>59</sup>, R. Paladini<sup>56</sup>, D. Paoletti<sup>49</sup>, B. Partridge<sup>43</sup>, F. Pasian<sup>47</sup>, G. Patanchon<sup>1</sup>, O. Perdereau<sup>71</sup>, L. Perotto<sup>75</sup>, F. Perrotta<sup>83</sup>, F. Piacentini<sup>32</sup>, M. Piat<sup>1</sup>, E. Pierpaoli<sup>22</sup>, S. Plaszczynski<sup>71</sup>, E. Pointecouteau<sup>88,8</sup>, G. Polenta<sup>3,46</sup>, N. Ponthieu<sup>59,52</sup>, L. Popa<sup>62</sup>, T. Poutanen<sup>44,24,2</sup>, G. W. Pratt<sup>73</sup>, S. Prunet<sup>60,87</sup>, J.-L. Puget<sup>59</sup>, J. P. Rachen<sup>20,78</sup>, W. T. Reach<sup>89</sup>, R. Rebolo<sup>66,13,39</sup>, M. Reinecke<sup>78</sup>, C. Renault<sup>75</sup>, S. Ricciardi<sup>49</sup>, T. Riller<sup>78</sup>, I. Ristorcelli<sup>88,8</sup>, G. Rocha<sup>68,9</sup>, C. Rosset<sup>1</sup>, M. Rowan-Robinson<sup>55</sup>, J. A. Rubiño-Martín<sup>66,39</sup>, B. Rusholme<sup>56</sup>, A. Sajina<sup>23</sup>, M. Sandri<sup>49</sup>, G. Savini<sup>82</sup>, D. Scott<sup>21</sup>, G. F. Smoot<sup>26,77,1</sup>, J.-L. Starck<sup>73</sup>, R. Sudiwala<sup>84</sup>, A.-S. Suur-Uski<sup>24,44</sup>, J.-F. Sygnet<sup>60</sup>, J. A. Tauber<sup>42</sup>, L. Terenzi<sup>49</sup>, L. Toffolatti<sup>18,67</sup>, M. Tomasi<sup>50</sup>, M. Tristram<sup>71</sup>, M. Tucci<sup>71</sup>, M. Türler<sup>53</sup>, L. Valenziano<sup>49</sup>, B. Van Tent<sup>76</sup>, P. Vielva<sup>67</sup>, F. Villa<sup>49</sup>, N. Vittorio<sup>36</sup>, L. A. Wade<sup>68</sup>, B. D. Wandelt<sup>60,87,29</sup>, M. White<sup>26</sup>, D. Yvon<sup>14</sup>, A. Zacchei<sup>47</sup>, and A. Zonca<sup>28</sup>

(Affiliations can be found after the references)

Submitted 19-Jul-2012 / Accepted ??

## Abstract

We make use of the *Planck* all-sky survey to derive number counts and spectral indices of extragalactic sources – infrared and radio sources – from the *Planck* Early Release Compact Source Catalogue at 100 to 857 GHz (3 mm to 350  $\mu$ m). Three zones (deep, medium and shallow) of approximately homogeneous coverage are used to ensure a clean completeness correction. Our sample, prior to the 80 % completeness cut, contains between 217 sources at 100 GHz and 1058 sources at 857 GHz over about 12,800 to 16,550 deg<sup>2</sup> (31 to 40 % of the sky). After the 80 % completeness cut, between 122 and 452 sources remain, with flux densities above 0.3 and 1.9 Jy. Using the multi-frequency coverage of the *Planck* High Frequency Instrument, all the sources have been classified into dust-dominated (infrared galaxies) or synchrotron-dominated (radio galaxies) spectral energy distributions (SED). We find an approximately equal number of synchrotron and dusty sources between 217 and 353 GHz; at 353 GHz or higher (respectively 217 GHz or lower) frequencies, the number is dominated by dusty (synchrotron) sources, as expected. For most of the sources, the spectral indices are also derived. We provide bright counts from 353 to 857 GHz and the contributions from dusty and synchrotron sources at all HFI frequencies, in the key spectral range where these spectra are crossing, for the first time in a coherent way. The observed counts are in the Euclidean regime. The number counts are compared to previously published data (from earlier *Planck* results, *Herschel*, BLAST, SCUBA, LABOCA, SPT, and ACT) and models. We derive the multi-frequency Euclidean level – the plateau in the normalised differential counts at high flux-density – and compare it to *WMAP*, *Spitzer* and *IRAS* results. The submillimetre number counts are not well reproduced by current evolution models of dusty galaxies, whereas the millimetre part appears reasonably well fitted by the most recent model for synchrotron-dominated sources. Finally we provide estimates of the local luminosity density of dusty galaxies, providing the first measurements at 545 and 857 GHz.

**Key words.** Cosmology: observations – Surveys – Galaxies: statistics – Galaxies: evolution – Galaxies: star formation – Galaxies: active – Radio continuum: galaxies – Submillimetre: galaxies

## 1. Introduction

Among other advantages, all-sky multifrequency surveys have the benefit of probing rare and/or bright objects in the sky. One

reason to probe bright objects is to study the number counts of extragalactic sources and their spectral shapes. In the far-infrared (FIR) the sources detected by these surveys are usually domi-

Planck 857 GHz mask and WMAP KQ75

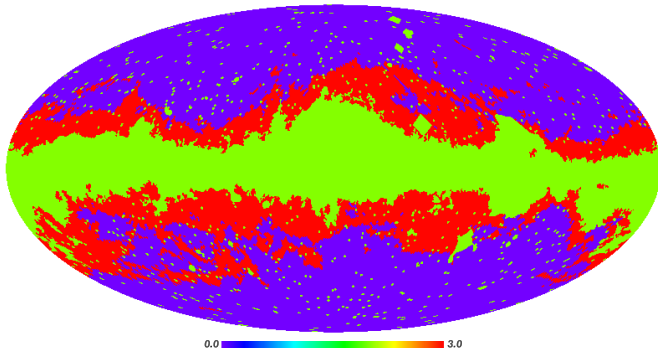


**Figure 1.** Comparison between our *Planck* 857 GHz mask (red means removed from the analysis) and *WMAP* 7-year KQ75 mask (green means removed); unlike the case for the mask employed in this paper, the *WMAP* mask excludes some point sources. The background (blue) is the sky area used for our analysis. This map is a Mollweide projection of the sky in Galactic coordinates.

nated by low-redshift galaxies with  $z < 0.1$ , e.g. *IRAS* at  $60\mu\text{m}$  (Ashby et al., 1996) but also reveal the presence of a few extreme objects like the lensed F10214 source (Rowan-Robinson et al., 1991). However, the radio range population is dominated by synchrotron sources (in particular, blazars) at higher redshift (see de Zotti et al., 2010, for a recent review). Previous multifrequency all-sky surveys were carried out in the infrared (IR) range by the *IRAS* satellite (between  $12$  and  $100\mu\text{m}$ ; Neugebauer et al. 1984), and more recently by *Akari* (between  $2$  and  $180\mu\text{m}$ ; Murakami et al. 2007) and *WISE* (between  $3.4$  and  $22\mu\text{m}$ ; Wright et al. 2010). They were carried out in the IR and microwave range by *COBE* (between  $1.2\mu\text{m}$  and  $1\text{cm}$ ; Boggess et al. 1992), and more recently in the microwave range by *WMAP* (between  $23$  and  $94\text{GHz}$ ; Bennett et al. 2003; Wright et al. 2009; Massardi et al. 2009; de Zotti et al. 2010).

At large flux densities (typically  $1\text{Jy}$  and above), FIR extragalactic number counts from all-sky surveys show a Euclidean component, i.e. a distribution of the number of source per flux density bin  $S_\nu$  at observed frequency  $\nu$  ( $dN/dS_\nu$  in  $\text{Jy sr}^{-1}$ ) proportional to  $S_\nu^{-2.5}$  (see Eq. 1) – in line with expectations from a local Universe uniformly filled with non-evolving galaxies (Lonsdale & Hacking, 1989; Hacking & Soifer, 1991; Bertin & Dennefeld, 1997; Massardi et al., 2009; Wright et al., 2009). In the radio range, the Euclidean part is modified by the presence of higher-redshift sources. At flux densities smaller than typically  $0.1$  to  $1\text{Jy}$ , an excess in the number counts compared to the Euclidean level is an indication of evolution in luminosity and/or density of the galaxy populations. This effect is clearly seen in deeper surveys in the FIR – e.g. (Genzel & Cesarsky, 2000; Dole et al., 2001, 2004; Frayer et al., 2006; Soifer et al., 2008; Bethérmin et al., 2010a) – in the submillimetre (submm) range – e.g. (Barger et al., 1999; Blain et al., 1999; Ivison et al., 2000; Greve et al., 2004; Coppin et al., 2006; Weiss et al., 2009; Patanchon et al., 2009; Clements et al., 2010; Lapi et al., 2011) – and millimetre and radio ranges – e.g. (de Zotti et al., 2010; Vieira et al., 2010; Vernstrom et al., 2011).

Planck 353 GHz mask and WMAP KQ85

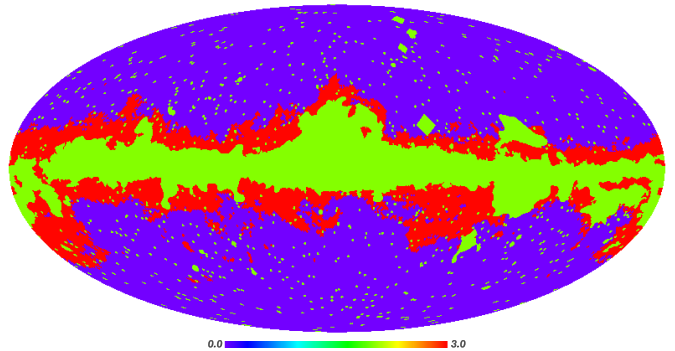


**Figure 2.** Comparison between our *Planck* 353 GHz mask (red means removed) and *WMAP* 7-year KQ85 mask (green means removed). The background (blue) is the sky area used for the analysis.

The *Planck*<sup>1</sup> all-sky survey covers nine bands between  $30$  and  $857\text{GHz}$ . It gives us for the first time robust extragalactic counts over a wide area of sky at these wavelengths, and the first all-sky coverage between  $3\text{mm}$  (*WMAP*) and  $160\mu\text{m}$  (*Akari*) – e.g. see Table 1 of Planck Collaboration VII (2011). The counts give us powerful constraints on the long-wavelength spectral energy distribution (SED) of the dusty galaxies investigated e.g. by *IRAS*, and on the short-wavelength SED of the active galaxies studied at radio wavelengths, e.g. by *WMAP* or ground-based facilities.

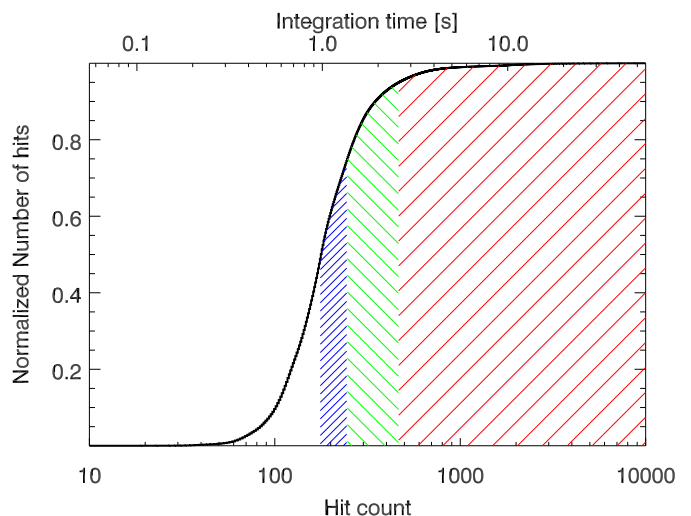


**Figure 3.** Cumulative distribution of *Planck* hit counts on the sky (here at  $857\text{GHz}$  with  $N_{\text{side}}=2048$ ), with the corresponding integration time per sky pixel (given in the top axis). The three sky zones used in the analysis are defined at  $857\text{GHz}$ : shallow (50 to 75 % of the hit count distribution, short-spaced lines, blue); medium (75 to 95 % of the hit counts, medium-spaced lines, green); and deep (95 % and above hits, widely-spaced lines, red).

<sup>1</sup> *Planck* (<http://www.esa.int/Planck>) is a project of the European Space Agency (ESA) with instruments provided by two scientific consortia funded by ESA member states (in particular the lead countries France and Italy), with contributions from NASA (USA) and telescope reflectors provided by a collaboration between ESA and a scientific consortium led and funded by Denmark.

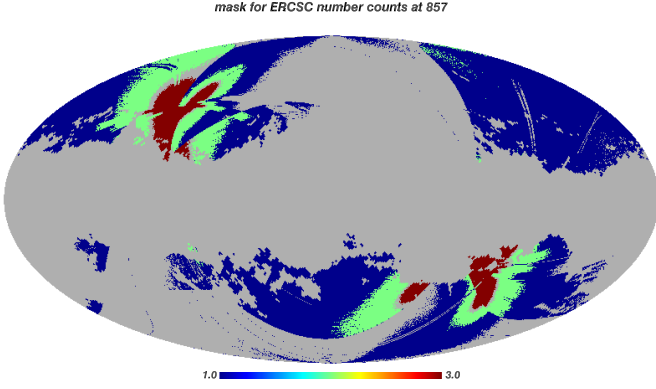


**Figure 4.** The three sky zones used in the analysis at 857 GHz: deep (red); medium (green); and shallow (blue); These are based on the 857 GHz hit counts.

We present here the extragalactic number counts and spectral indices of galaxies selected at high Galactic latitude and using identifications, detected at the six highest *Planck* frequencies, between 100 and 857 GHz. *Planck* number counts and spectral indices of extragalactic radio-selected sources were already published for the frequency range 30 to 217 GHz using LFI and HFI instruments (Planck Collaboration XIII, 2011). The transition between synchrotron-dominated sources and thermal dust-dominated occurs in the crucial spectral range 200–800 GHz. Thus our broad frequency data allow a better spectral characterisation, useful for estimating e.g. the point source contamination. *Planck* has the unique capability to study both populations, taking advantage of its wide spectral and all-sky coverage.

We use the *WMAP* 7 year best-fit  $\Lambda$ CDM cosmology (Larson et al., 2011), with  $H_0 = 71 \text{ km s}^{-1} \text{ Mpc}^{-1}$ ,  $\Omega_\Lambda = 0.734$  and  $\Omega_M = 0.266$ .

## 2. *Planck* data, masks and sources

*Planck* (Tauber et al., 2010; Planck Collaboration I, 2011) is the third generation space mission to measure the anisotropy of the cosmic microwave background (CMB). It observes the sky in nine frequency bands covering 30–857 GHz with high sensitivity and angular resolution from  $31'$  to  $5'$ . The Low Frequency Instrument LFI; (Mandolesi et al., 2010; Bersanelli et al., 2010; Mennella et al., 2011) covers the 30, 44, and 70 GHz bands with amplifiers cooled to 20 K. The High Frequency Instrument (HFI; Lamarre et al. 2010; Planck HFI Core Team 2011a) covers the 100, 143, 217, 353, 545, and 857 GHz bands with bolometers cooled to 0.1 K. Polarization is measured in all but the highest two bands (Leahy et al., 2010; Rosset et al., 2010). A combination of radiative cooling and three mechanical coolers produces the temperatures needed for the detectors and optics (Planck Collaboration II, 2011). Two Data Processing Centers (DPCs) check and calibrate the data and make maps of the sky (Planck HFI Core Team, 2011b; Zacchei et al., 2011). *Planck*'s sensitivity, angular resolution, and frequency coverage make it a powerful instrument for galactic and extragalactic astrophysics as well as cosmology. Early astrophysics results are given in Planck Collaboration VIII–XXVI 2011, based on data taken between 13 August 2009 and 7 June 2010. Intermediate astrophysics results are now being presented in a series of papers based on data taken between 13 August 2009 and 27 November 2010.

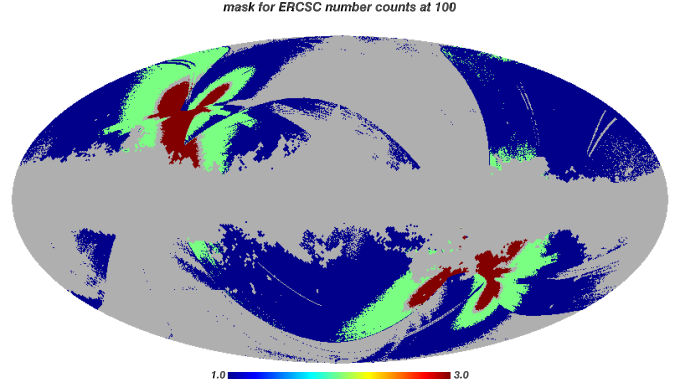


**Figure 5.** The three sky zones used in the analysis at 100 GHz: deep (red); medium (green); and shallow (blue). These are based on the 100 GHz hit counts.

The *Planck* data used in this paper (unlike other intermediate *Planck* papers) correspond to the first 1.6 sky surveys (Planck Collaboration I, 2011; Planck HFI Core Team, 2011a,b), from which the Early Release Compact Source Catalogue, or ERCSC (Planck Collaboration VII, 2011; Planck Collaboration, 2011) has been extracted and documented. First results from the ERCSC are published as *Planck* early papers (Planck Collaboration XIII, 2011; Planck Collaboration XIV, 2011; Planck Collaboration XV, 2011; Planck Collaboration XVI, 2011). We use HFI data, covering the 100–857 GHz range in six bands.

### 2.1. Galactic masks

To obtain reliable extragalactic number counts, uncontaminated by Galactic sources, we mask out areas of the sky strongly affected by Galactic sources, defining a set of “Galactic masks”. These are based on removing a fraction of the sky above a specified level in sky surface brightness. We use two masks, one at high frequencies (857 and 545 GHz), and one at lower frequen-

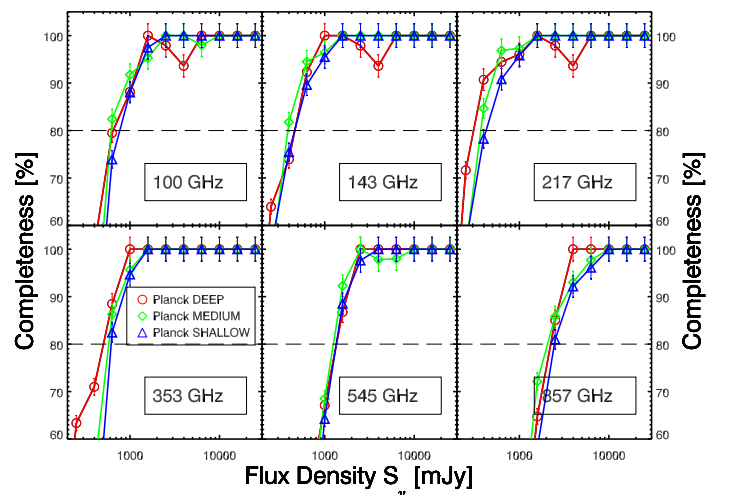


**Figure 6.** Completeness (vs. flux density of sources) coming from the Monte-Carlo runs for the ERCSC and derived for each zone. The horizontal dashed line represents our threshold for number count analysis.



cies (353 GHz and below). The use of two different masks is motivated by the different astrophysical components dominating the higher HFI frequencies and the lower frequencies, which are not necessarily spatially correlated. While the Galactic dust dominates at 857 GHz, its spectrum decreases with decreasing frequency. On the contrary, the synchrotron and free-free components dominate at 100 GHz.

Before applying a brightness cut to the maps, we degrade the angular resolution of the maps from  $1'.5$  ( $N_{\text{side}}=2048$  in HEALPIX; Górski et al. 2005) down to  $55'$  ( $N_{\text{side}}=64$ ). The maps at low resolution are then interpolated at the original high angular resolution. Creating a Galactic mask using this procedure has the double benefit of: 1) not masking the bright sources (because they are smoothed); and 2) smoothing the Galactic structure.

The 857 GHz Galactic mask keeps 48 % of the sky for analysis (thus removing 52 % of the sky), and this corresponds to a cut of  $2.2 \text{ MJy sr}^{-1}$  at 857 GHz. This mask is applied at 857 and 545 GHz. The 353 GHz Galactic mask keeps 64 % of the sky for analysis (thus removing 36 % of the sky), and corresponds to a cut of  $0.28 \text{ MJy sr}^{-1}$  at 353 GHz. This mask is applied at 353, 217, 143 and 100 GHz.

Figs. 1 and 2 show the *Planck* masks, comparing them with the *WMAP* 7 year KQ75 and KQ85 masks (Gold et al., 2011; Jarosik et al., 2011). Notice that we do not use the *WMAP* masks in this work.

## 2.2. Three zones in the sky: deep, medium and shallow

Three main zones are identified to ensure homogeneous coverage of the sky by the *Planck* detectors at each frequency, thereby allowing a subsequent estimate of the completeness. The *Planck* data used here correspond to approximately 1.6 complete surveys of the sky and have a non-uniform coverage (Planck Collaboration I, 2011; Planck HFI Core Team, 2011a,b). While performing statistics on sources drawn from a non-uniformly covered survey is feasible, the nature of the *Planck* data (including scanning strategy, and masking of planets – see ERCSC article Planck Collaboration VII 2011) and its heterogeneous coverage (by a factor more than  $10^3$ , see Fig. 3) – make it difficult to implement. We therefore select three zones in the sky, in each of which the observations are approximately homogeneous in integration time.

We define the hit count by counting the number of times a single *Planck* detector observes one sky position in the sky. The hit count can also be defined for a frequency band: it is the number of times each sky pixel has been hit by any *Planck* detector at a given frequency. We will be using this latter definition. This quantity is similar to  $N_{\text{obs}}$  in *WMAP* data files.

The three zones have hit counts varying by not more than a factor of two, except in the smaller deep zone (at the ecliptic poles) where there is high redundancy. They are defined as (and illustrated in Fig. 3):

- deep: 95 % or more of the cumulative hit count distribution at a given frequency;
- medium: 75 to 95 % of the cumulative hit count distribution at a given frequency;
- shallow: 50 to 75 % of the cumulative hit count distribution at a given frequency.

Thus, pixels in the deep zone (at a given frequency) all have a hit count value greater than or equal to the hit count value corresponding to 95 % of the total distribution at this frequency. Notice that each frequency map has different hit counts, due

to the focal plane geometry; each zone will thus have slight differences in geometry from one frequency to another, leading to slightly different surface areas. Table 2 summarizes the surface area of each zone (deep, medium and shallow); typically, the deep zone covers  $1000 \text{ deg}^2$ , the medium zone about  $3000 \text{ deg}^2$ , and the shallow about  $12000 \text{ deg}^2$ . Fig. 4 (5, respectively) represents the three different zones used in this analysis: deep, medium and shallow at 857 GHz (100 GHz, respectively).

## 2.3. Sample selection and validation

The sample is drawn from the first public catalogue of *Planck* sources, the ERCSC (Planck Collaboration VII, 2011), containing highly reliable sources. The selection is performed with the following steps at each HFI frequency independently:

- select sources within each zone: deep, medium and shallow;
- select point sources, using the keyword “EXTENDED” set to zero;

These criteria should favour the presence of galaxies rather than Galactic sources. To validate this, we make three checks in addition to using conservative masks.

1. We measure the mid-IR vs. submm flux density ratios of known Galactic cold cores (from the *Planck* Early Cold Core catalogue, ECC, Planck Collaboration XXIII 2011) and conversely of known galaxies of the ERCSC. Using *WISE* (Wright et al., 2010) W3 and W4 bands (when available with the first public release), and the 857 GHz HFI band, we measure a factor of 100 to 200 between the submm-to-mid-infrared ratios of galaxies and ECC sources. When measuring this ratio in our sample, we see that the submm-to-mid-infrared colours of sources in our sample are compatible with galaxy colours, and not with ECC colours.

2. The CIRRUS flag in the ERCSC gives an estimate of the normalised neighbour surface density of sources at 857 GHz, as a proxy for a cirrus estimate. The median value of the CIRRUS flag in our sample is 0.093 at 857 GHz, a low value compatible with no cirrus contamination when used in conjunction with the EXTENDED=0 flag (e.g. Herranz et al. 2012).

3. We query the NED and SIMBAD databases at the positions of all our ERCSC sources using a  $2'.5$  radius search. Each *Planck* source has many matches (many of them completely unrelated, e.g. foreground stars), and the identification is more complex at higher frequencies. However, as seen later with the counts estimates, our  $N(> S)$  cumulative distribution of sources is always less than 200 sources per steradian, i.e. less than  $3.3 \times 10^{-4}$  ERCSC sources per  $2'.5$  search radius on average.

We thus search for the most probable match by identifying the source type in the order Galactic, then extragalactic. The Galactic types include supernova remnants, planetary nebulae, nebulae, HII regions, stars, molecular clouds, globular/star clusters. We call a source “Galactic unsecure” when one of the two databases returns no identification and the other a Galactic identification. We do not use “Galactic secure” or “Galactic unsecure” sources in this paper. The statistics of identifications is given in Table 1.

Our final sample is composed of confirmed galaxies, the vast majority being NGC, *IRAS*, radio sources and blazar objects, as well as some unidentified sources (a small fraction of the total number). These completely unidentified sources, where no SIMBAD or NED ID was found, are interpreted as potential galaxies, and hence are included in our counts, because they have a small cirrus flag value (see point 2 above),

**Table 1.** Percentage of *Planck* source identifications using the SIMBAD and NED databases (with the number of sources in parentheses).

$\nu$ [GHz]	Extragalactic Secure % (Nb.)	Galactic Unsecure % (Nb.)	Galactic Secure % (Nb.)	Unidentified % (Nb.)	Total % (Nb.)
857 deep	91.2 (73)	2.5 (2)	1.2 (1)	5.0 (4)	100 (80)
857 medium	95.5 (255)	1.9 (5)	0.0 (0)	2.6 (7)	100 (267)
857 shallow	94.6 (697)	1.6 (12)	0.8 (6)	3.0 (22)	100 (737)
545 deep	76.5 (39)	7.8 (4)	2.0 (1)	13.7 (7)	100 (51)
545 medium	91.1 (143)	2.5 (4)	0.0 (0)	6.4 (10)	100 (157)
545 shallow	91.8 (301)	2.1 (7)	0.9 (3)	5.2 (17)	100 (328)
353 deep	81.6 (31)	2.6 (1)	5.3 (2)	10.5 (4)	100 (38)
353 medium	87.0 (94)	0.9 (1)	2.8 (3)	9.3 (10)	100 (108)
353 shallow	78.0 (170)	4.6 (10)	4.6 (10)	12.8 (28)	100 (218)
217 deep	77.3 (17)	0.0 (0)	22.7 (5)	0.0 (0)	100 (22)
217 medium	92.5 (62)	1.5 (1)	1.5 (1)	4.5 (3)	100 (67)
217 shallow	88.5 (170)	0.5 (1)	4.2 (8)	6.8 (13)	100 (192)
143 deep	86.7 (13)	0.0 (0)	13.3 (2)	0.0 (0)	100 (15)
143 medium	100.0 (48)	0.0 (0)	0.0 (0)	0.0 (0)	100 (48)
143 shallow	96.8 (182)	0.5 (1)	1.6 (3)	1.1 (2)	100 (188)
100 deep	77.8 (14)	0.0 (0)	22.2 (4)	0.0 (0)	100 (18)
100 medium	100.0 (45)	0.0 (0)	0.0 (0)	0.0 (0)	100 (45)
100 shallow	93.9 (154)	0.0 (0)	3.7 (6)	2.4 (4)	100 (164)

**Table 2.** Number of extragalactic ERCSC sources in our sample prior to the completeness cut (and after the completeness cut in parentheses), together with the surface area of the zones.

$\nu$ [GHz]	number deep	number medium	number shallow	total source number	surface area deep	surface area medium	surface area shallow	total surface [deg <sup>2</sup> ]
857	77 (24)	262 (115)	719 (313)	1058 (452)	880	2288	9800	12969
545	46 (8)	153 (69)	318 (143)	517 (220)	874	2324	9551	12749
353	35 (14)	104 (59)	198 (151)	337 (224)	1086	2971	12373	16431
217	17 (15)	65 (57)	183 (71)	265 (143)	1104	3169	11900	16174
143	13 (8)	48 (44)	184 (90)	245 (142)	1111	2972	11977	16061
100	14 (6)	45 (39)	158 (77)	217 (122)	1072	2870	12611	16554

**Table 3.** Number of extragalactic ERCSC sources actually used in the number counts: deep – medium – shallow, with the numbers of unidentified sources after the slash.

$\langle S_\nu \rangle$ [Jy]	$S_\nu$ [Jy]	range	857 GHz	545 GHz	353 GHz	217 GHz	143 GHz	100 GHz
0.398	0.303	– 0.480	0	0	0	7/0 - 28/1 - 92/9	3/0 - 12/0 - 81/1	0
0.631	0.480	– 0.762	0	0	8/0 - 31/4 - 83/14	3/0 - 13/1 - 34/2	2/0 - 13/0 - 43/0	4/0 - 15/0 - 68/3
1.000	0.762	– 1.207	0	0	4/0 - 18/2 - 38/7	4/0 - 8/0 - 21/1	4/0 - 10/0 - 25/0	4/0 - 11/0 - 47/1
1.585	1.207	– 1.913	0	5/0 - 26/6 - 78/9	1/1 - 6/0 - 14/0	1/0 - 4/0 - 11/0	2/0 - 4/0 - 12/0	2/0 - 7/0 - 13/0
2.512	1.913	– 3.032	11/0 - 31/1 - 139/4	0/0 - 20/1 - 28/1	1/0 - 2/0 - 8/0	0/0 - 1/0 - 3/0	0/0 - 3/0 - 5/0	0/0 - 3/0 - 11/0
3.981	3.032	– 4.805	7/0 - 33/2 - 95/4	1/0 - 16/1 - 20/1	0/0 - 1/0 - 6/0	0/0 - 2/0 - 1/0	0/0 - 1/0 - 3/0	0/0 - 2/0 - 3/0
6.310	4.805	– 7.615	3/0 - 22/2 - 41/7	1/0 - 6/0 - 8/1	0	0/0 - 1/0 - 1/0	0/0 - 1/0 - 1/0	0/0 - 0/0 - 2/0
10.000	7.615	– 12.069	2/0 - 20/1 - 23/1	1/0 - 1/0 - 5/0	0/0 - 1/0 - 0/0	0	0/0 - 0/0 - 1/0	0/0 - 1/0 - 1/0
15.849	12.069	– 22.801	1/0 - 9/0 - 15/0	0/0 - 0/0 - 4/0	0/0 - 0/0 - 2/0	0	0	0

Table 2 summarises the source number and surface area of each zone (deep, medium and shallow). We find a total number of sources ranging from 217 at 100 GHz to 1058 at 857 GHz.

#### 2.4. Completeness

The ERCSC Pipeline (Planck Collaboration VII, 2011) used extensive Monte-Carlo simulations to assess various parameters such as positional or flux density accuracies. Here, we use the results of those runs to estimate the completeness in each of the

three zones presented in Fig. 6. The uncertainties in completeness are at the 5 % level, as discussed in Planck Collaboration VII (2011) and Planck Collaboration (2011). The correction for incompleteness is then applied to the number counts of each zone separately.

We will use a completeness level threshold of 80 % for all frequencies. This ensures: 1) a minimal source contamination; 2) no photometric biases (Planck Collaboration, 2011); and 3) good photometric accuracy (Planck Collaboration, 2011) – see Sect. 2.5. The number of sources actually used to estimate the

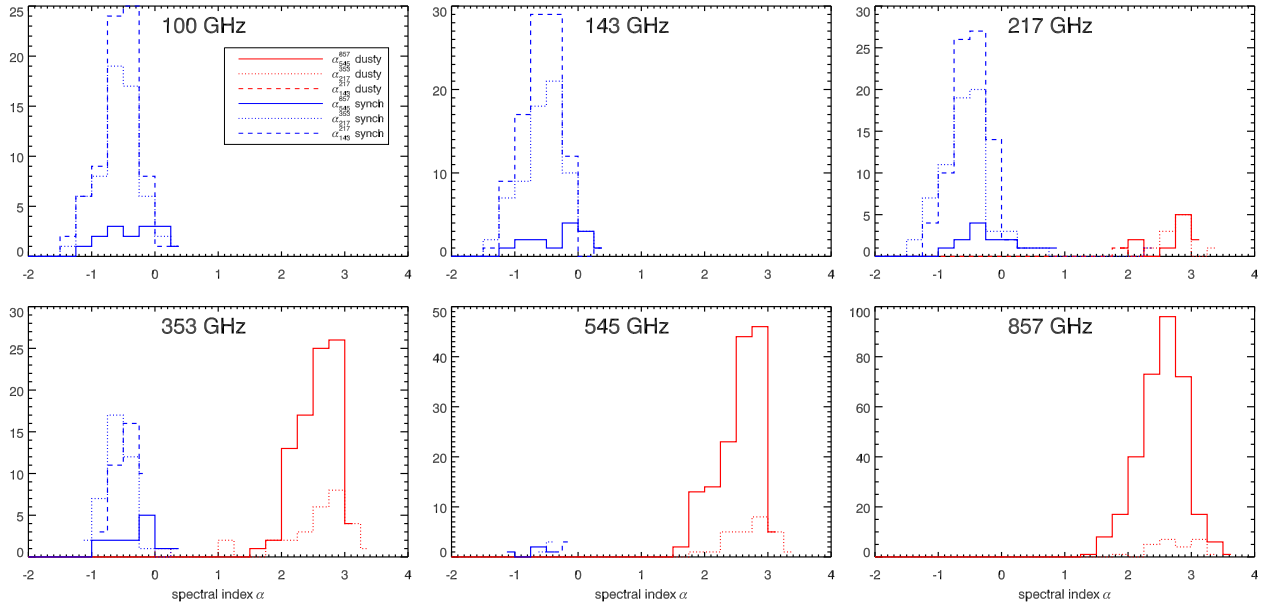


**Figure 7.** Distribution of spectral indices (for the sources present in the ERCSC at a given frequency in our sample with completeness of 80 % or above). Here  $\alpha_{143}^{217}$  is shown as a dotted line,  $\alpha_{217}^{353}$  as a dashed line, and  $\alpha_{545}^{857}$  as a solid line. The region  $2 \leq \alpha \leq 4$  is typical of thermal dust emission. In red we show the dusty sources, whereas in blue we show the synchrotron sources. The sources in all three samples (deep, medium, and shallow) are combined here. Note that, as expected, the 100 GHz, and 143 GHz samples are dominated by radio galaxies, whereas the 545 GHz and 857 GHz samples are dominated by dusty galaxies. At 217 GHz and 353 GHz we observe the transition between the two populations, with significant numbers of both types being present in the samples.

number counts is given in Tab. 3, which also includes the number of unidentified sources. We finally use a number of sources ranging from 122 at 100 GHz to 452 at 857 GHz (Tab. 2).

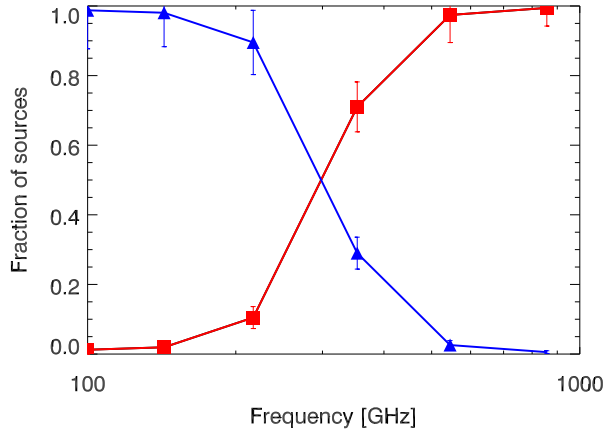


**Figure 8.** Fraction of galaxy types as a function of frequency, on the sample having completeness of 80 % and above: dusty (red squares) and synchrotron (blue triangles). Error bars are Poissonian.

## 2.5. Photometry

The photometry of the ERCSC is extensively detailed in [Planck Collaboration VII \(2011\)](#) as well as in the explanatory supple-

ment [Planck Collaboration \(2011\)](#). Here we use the “FLUX” field for flux densities. Notice that 100 and 217 GHz flux densities can be affected by Galactic CO lines ([Planck HFI Core Team, 2011b](#)).

We would like to emphasise that the extensive simulations performed in the process of generating/validating the ERCSC allow us to derive reliable completeness estimates for each zone (see Sect. 2.4) and also to estimate the quality of the photometry. In the faintest flux density bins that we are using (corresponding to 80 % completeness), there is no photometric offset, and the photometric accuracy from the Monte-Carlo simulations is about ([Planck Collaboration, 2011](#), ; Fig. 7 for reference): 35 % at 480 mJy for 100 GHz; 30 % at 300 mJy for 143 GHz; 20 % at 300 mJy for 217 GHz; 20 % at 480 mJy for 353 GHz; 20 % at 1207 mJy for 545 GHz; and 20 % at 1913 mJy for 857 GHz. This scatter (in the faintest flux density bins) strongly decreases at larger flux densities. Notice that photometric uncertainties can bias the determination of the counts slope (e.g. [Murdoch, Crawford & Jauncey, 1973](#)).

From our sample, we also create “Band-filled catalogues”. For each frequency/zone sample, we take each source position from the ERCSC and perform aperture photometry from the corresponding images in the other frequencies. We adopt  $4\sigma$  as the detection threshold. These aperture photometry measurements (and upper limits) are used for the spectral classification of sources and in the spectral index determinations, but not in the number counts measurements (which rely only on ERCSC flux densities). We define the spectral index  $\alpha$  by  $S_\nu \propto \nu^\alpha$ .

The derived spectral indices are used to determine the colour correction of the ERCSC flux densities ([Planck HFI Core Team, 2011b](#)). This correction changes the flux densities by at most 5 % at 857 GHz, 15 % at 545 GHz, 14 % at 353 GHz, 12 % at 217 GHz, and 1 % at 143 GHz and 100 GHz.

**Table 4.** *Planck* number counts at 353, 545 and 857 GHz.

$\langle S_\nu \rangle$ [Jy]	$S_\nu$ [Jy]	range	$dN/dS_{857} S_{857}^{2.5}$ [Jy <sup>1.5</sup> sr <sup>-1</sup> ]	$N > S_{857}$ [sr <sup>-1</sup> ]	$dN/dS_{545} S_{545}^{2.5}$ [Jy <sup>1.5</sup> sr <sup>-1</sup> ]	$N > S_{545}$ [sr <sup>-1</sup> ]	$dN/dS_{353} S_{353}^{2.5}$ [Jy <sup>1.5</sup> sr <sup>-1</sup> ]	$N > S_{353}$ [sr <sup>-1</sup> ]
0.631	0.480	– 0.762	0	0	0	0	30.6 ± 3.7	50.1 ± 3.3
1.000	0.762	– 1.207	0	0	0	0	26.4 ± 4.0	21.0 ± 2.1
1.585	1.207	– 1.913	0	0	131.4 ± 21.4	60.3 ± 4.1	17.6 ± 4.1	8.4 ± 1.3
2.512	1.913	– 3.032	466.2 ± 70.5	127.7 ± 6.0	104.6 ± 20.4	28.9 ± 2.7	18.3 ± 5.7	4.2 ± 0.9
3.981	3.032	– 4.805	613.6 ± 96.6	71.8 ± 4.4	160.2 ± 33.8	16.3 ± 2.1	23.3 ± 9.0	2.0 ± 0.6
6.310	4.805	– 7.615	573.4 ± 103.4	35.0 ± 3.0	129.4 ± 37.5	6.7 ± 1.3	0	0
10.000	7.615	– 12.069	755.2 ± 150.3	17.7 ± 2.1	119.5 ± 47.8	2.8 ± 0.9	13.2 ± 13.3	0.6 ± 0.3
15.849	12.069	– 22.801	837.1 ± 200.5	6.3 ± 1.3	136.2 ± 70.4	1.0 ± 0.5	52.9 ± 37.6	0.4 ± 0.3

**Table 5.** *Planck* number counts at 100, 143 and 217 GHz.

$\langle S_\nu \rangle$ [Jy]	$S_\nu$ [Jy]	range	$dN/dS_{217} S_{217}^{2.5}$ [Jy <sup>1.5</sup> sr <sup>-1</sup> ]	$N > S_{217}$ [sr <sup>-1</sup> ]	$dN/dS_{143} S_{143}^{2.5}$ [Jy <sup>1.5</sup> sr <sup>-1</sup> ]	$N > S_{143}$ [sr <sup>-1</sup> ]	$dN/dS_{100} S_{100}^{2.5}$ [Jy <sup>1.5</sup> sr <sup>-1</sup> ]	$N > S_{100}$ [sr <sup>-1</sup> ]
0.398	0.303	– 0.480	16.5 ± 2.0	54.3 ± 3.54	8.5 ± 1.1	44.3 ± 2.95	0	0
0.631	0.480	– 0.762	11.5 ± 1.9	23.0 ± 2.21	13.7 ± 2.1	28.1 ± 2.46	21.9 ± 3.0	43.7 ± 3.14
1.000	0.762	– 1.207	14.6 ± 2.8	12.0 ± 1.58	17.4 ± 3.1	15.0 ± 1.77	29.1 ± 4.4	22.9 ± 2.22
1.585	1.207	– 1.913	13.6 ± 3.6	5.1 ± 1.01	15.4 ± 3.8	6.7 ± 1.17	18.8 ± 4.3	9.1 ± 1.35
2.512	1.913	– 3.032	6.8 ± 3.4	1.8 ± 0.61	13.6 ± 5.0	3.1 ± 0.79	23.2 ± 6.5	4.6 ± 0.95
3.981	3.032	– 4.805	10.1 ± 5.9	1.0 ± 0.45	13.6 ± 6.9	1.4 ± 0.54	16.5 ± 7.5	1.8 ± 0.59
6.310	4.805	– 7.615	13.5 ± 9.6	0.4 ± 0.29	13.6 ± 9.7	0.6 ± 0.35	13.2 ± 9.4	0.8 ± 0.40
10.000	7.615	– 12.069	0	0	13.6 ± 13.6	0.2 ± 0.20	26.3 ± 18.7	0.4 ± 0.28

### 3. Classification of galaxies into dusty or synchrotron categories

For the purposes of this paper, we aim for a basic classification based on SEDs that separates sources into those dominated by thermal dust emission and those dominated by synchrotron emission. (Free-free emission does exist, but is not dominant, e.g., [Peel et al. 2011](#)). In order to classify our sources by type, we start with the band-filled catalogues discussed in Section 2.5. Thermal dust emission is expected to show spectral indices in the range  $\alpha \sim 2-4$ . On the other hand, colder temperature sources can show lower  $\alpha_{545}^{857}$ , if the 857 GHz point is near the spectral peak. The presence of a strong synchrotron component, or perhaps free-free emission component, would start to flatten the SED below  $\sim 353$  GHz. With such issues in mind, we have set up the following classification algorithm:

- all sources with  $\alpha_{545}^{857} \geq 2$ , or  $\alpha_{353}^{545} \geq 2$  are assigned a “dusty” classification;
- all sources where both of these spectral indices are lower than 2, including non-detections, are assigned “synchrotron” classification.

The resulting classification is summarised in Fig. 7, showing the spectral index distributions for each type as a function of observed frequency.

However, some sources are difficult to classify, and could be part of an “intermediate dusty” or “intermediate synchrotron” type. These intermediate sources can be defined as follows:

- being dusty (according to our criterion above) but also having  $\alpha_{100}^{857} < 1$
- being synchrotron (according to our criterion above) but also with  $\alpha_{30}^{70}$  measurable (using LFI data), i.e. sources that show both a significant dust component and a strong synchrotron component.

Among the sources included in the number counts analysis, fewer than 10 % are classified as “intermediate”. This frac-

tion rises significantly if we remove the completeness cut due to the increasing photometric uncertainties at lower flux densities (see Appendix A for details). Examples of both “dusty” or “synchrotron” sources with somewhat unusual SEDs are discussed in Appendix B.

### 4. *Planck* extragalactic number counts between 100 and 857 GHz

The *Planck* extragalactic number counts (differential, normalised to the Euclidean slope, and completeness-corrected) are presented in Fig. 9 and Tables 4 and 5. They are obtained using a mean of the 3 zones (weighted by the surface area of each zone).

The error budget in the number counts is made up of: (i) Poisson statistics (ii); the 5 % uncertainty in the completeness correction (iii); the absolute photometric calibration uncertainty of 2 % at and below 353 GHz, and 7 % above 545 GHz ([Planck HFI Core Team, 2011a,b](#)). According to e.g. Eq. 1 of [Bethérmin et al. \(2011\)](#), the calibration uncertainties scale to the power of 1.5 for Euclidean normalised number counts.

Notice that our bright counts error budget is dominated by sample variance at low redshift and by small-number statistics. For instance, the small wiggle seen in the counts at the three highest frequencies (seen at 600 mJy at 353 GHz, 4 Jy at 545 GHz and 10 Jy at 857 GHz) is due to a few tens of local NGC sources in the medium zone (see Appendices B and C).

Integral (i.e. cumulative) combined number counts are shown in Fig. 11. Although error bars are highly correlated, these counts provide a useful estimate of the source surface density. The completeness correction is also applied here, and we use the same cuts in flux density as for the differential counts. Tab. 4 and 5 also give the  $N > S$  values.



**Table 6.** *Planck* number counts of dusty galaxies (only) between 217 and 857 GHz.

$\langle S_\nu \rangle$ [Jy]	$S_\nu$ [Jy]	range	$dN/dS_{857}S_{857}^{2.5}$ [Jy <sup>1.5</sup> sr <sup>-1</sup> ]	$dN/dS_{545}S_{545}^{2.5}$ [Jy <sup>1.5</sup> sr <sup>-1</sup> ]	$dN/dS_{353}S_{353}^{2.5}$ [Jy <sup>1.5</sup> sr <sup>-1</sup> ]	$dN/dS_{217}S_{217}^{2.5}$ [Jy <sup>1.5</sup> sr <sup>-1</sup> ]
0.398	0.303	– 0.480	0	0	0	3.2 ± 0.7
0.631	0.480	– 0.762	0	0	23.6 ± 3.1	2.3 ± 0.8
1.000	0.762	– 1.207	0	0	18.5 ± 3.2	1.8 ± 0.9
1.585	1.207	– 1.913	0	129.0 ± 21.1	12.5 ± 3.4	0
2.512	1.913	– 3.032	463.6 ± 70.2	100.3 ± 19.8	11.7 ± 4.5	1.7 ± 1.7
3.981	3.032	– 4.805	609.0 ± 96.0	151.5 ± 32.5	13.3 ± 6.7	0
6.310	4.805	– 7.615	573.4 ± 103.4	129.4 ± 37.5	0	0
10.000	7.615	– 12.069	755.2 ± 150.3	119.5 ± 47.8	13.2 ± 13.3	0
15.849	12.069	– 22.801	837.1 ± 200.5	136.2 ± 70.4	26.4 ± 26.5	0

**Table 7.** *Planck* number counts of (only) synchrotron galaxies between 100 and 857 GHz.

$\langle S_\nu \rangle$ [Jy]	$S_\nu$ [Jy]	range	$dN/dS_{857}S_{857}^{2.5}$ [Jy <sup>1.5</sup> sr <sup>-1</sup> ]	$dN/dS_{545}S_{545}^{2.5}$ [Jy <sup>1.5</sup> sr <sup>-1</sup> ]	$dN/dS_{353}S_{353}^{2.5}$ [Jy <sup>1.5</sup> sr <sup>-1</sup> ]	$dN/dS_{217}S_{217}^{2.5}$ [Jy <sup>1.5</sup> sr <sup>-1</sup> ]	$dN/dS_{143}S_{143}^{2.5}$ [Jy <sup>1.5</sup> sr <sup>-1</sup> ]	$dN/dS_{100}S_{100}^{2.5}$ [Jy <sup>1.5</sup> sr <sup>-1</sup> ]
0.398	0.303	– 0.480	0	0	0	13.3 ± 1.7	8.5 ± 1.1	0
0.631	0.480	– 0.762	0	0	7.0 ± 1.4	9.2 ± 1.6	13.5 ± 2.1	21.9 ± 3.0
1.000	0.762	– 1.207	0	0	7.9 ± 2.0	12.8 ± 2.6	16.9 ± 3.1	28.6 ± 4.3
1.585	1.207	– 1.913	0	2.4 ± 1.7	5.0 ± 2.1	13.6 ± 3.6	15.4 ± 3.8	18.8 ± 4.3
2.512	1.913	– 3.032	2.6 ± 2.6	4.3 ± 3.1	6.7 ± 3.4	5.1 ± 3.0	13.6 ± 5.0	23.2 ± 6.5
3.981	3.032	– 4.805	4.5 ± 4.6	8.7 ± 6.2	10.0 ± 5.8	10.1 ± 5.9	13.6 ± 6.9	16.5 ± 7.5
6.310	4.805	– 7.615	0	0	0	13.5 ± 9.6	13.6 ± 9.7	13.2 ± 9.4
10.000	7.615	– 12.069	0	0	0	0	13.6 ± 13.6	26.3 ± 18.7
15.849	12.069	– 22.801	0	0	26.4 ± 26.5	0	0	0

## 5. Results & Discussion

### 5.1. Nature of the Galaxies at submillimetre and millimetre wavelengths

The change in the nature of sources (synch vs dusty) with frequency was first observed in the *Planck* data in [Planck Collaboration VII \(2011\)](#). Our new sample allows a more precise quantification because of its completeness. The statistics of synchrotron vs. dusty galaxies are summarised in Fig. 8, showing the fraction of galaxy type as a function of frequency. We estimate the uncertainty in the classification to be of the order of 10 % (see Appendix A). The striking result is the almost equal contribution of both source types near 300 GHz. The high frequency channels (545 and 857 GHz) are, unsurprisingly, dominated (> 90 %) by dusty galaxies. The low frequency channels are, unsurprisingly, dominated (> 95 %) by synchrotron sources at 100 and 143 GHz. At 217 GHz, fewer than 10 % of the sources show a dust-dominated SED.

All the sources from our complete sample have an identified spectral type (by construction), and we can compute the number counts for synchrotron and dusty galaxies. Fig. 9, 10 and 11 show the differential and integral number counts by type, also given in Tables 6 and 7. We note that at 353 GHz, about two thirds of the number counts are made-up by dusty sources. At 217 GHz (545 GHz) there is a minor contribution (10 % or less) of the dusty (synchrotron) sources contributing to the counts. These number counts of extragalactic dusty and synchrotron sources are an important step to further constrain models of galaxy SED and to include them in more general models of galaxy evolution (see below).

### 5.2. Planck Number Counts Compared with Other Datasets

The number counts are in fairly good agreement at lower frequencies (100 to 217 GHz) with the counts published in the *Planck* early results, based on a 30 GHz selected sample ([Planck Collaboration XIII, 2011](#)), represented as diamonds in Fig. 9 and 10. The effect of the completeness correction is seen in the fainter flux density bins, below about 500 mJy. However, we notice a slight disagreement around 400 mJy at 217 GHz, where our counts of synchrotron galaxies exceed the *Planck* early counts by a factor of 1.7 ( $13.7 \pm 1.5$  vs.  $8.2 \pm 0.9$  Jy<sup>1.5</sup> sr<sup>-1</sup>). This discrepancy can be easily understood: our current selection of synchrotron sources is not the same as the one adopted in the *Planck* Early results paper [Planck Collaboration XIII \(2011\)](#), in which a more restrictive criterion was used ( $\alpha_{143}^{217} < 0.5$ ). If we adopt the same criterion as in that paper we find no statistically significant difference between the two estimates of the number counts.

Our counts estimate also seem consistent with the *Herschel* ATLAS and HerMES counts ([Clements et al., 2010](#); [Oliver et al., 2010](#)) at high frequency (545 and 857 GHz) as well as BLAST at the same two wavelengths ([Bethemín et al., 2010b](#)), although there is no direct overlap in flux density and small number statistics affect the brightest *Herschel* points.

The ACT 148 GHz data ([Marriage et al., 2011](#)) and SPT 150 and 220 GHz ([Vieira et al., 2010](#)) are also plotted in Fig. 10, together with SCUBA and LABOCA data at 353 GHz ([Borys et al., 2003](#); [Coppin et al., 2006](#); [Scott et al., 2006](#); [Beelen et al., 2008](#); [Weiss et al., 2009](#)), covering more than four orders of magnitude in flux density.

We finally checked that our counts are in agreement with the *Planck* Sky Model ([Delabrouille et al., 2012](#)).



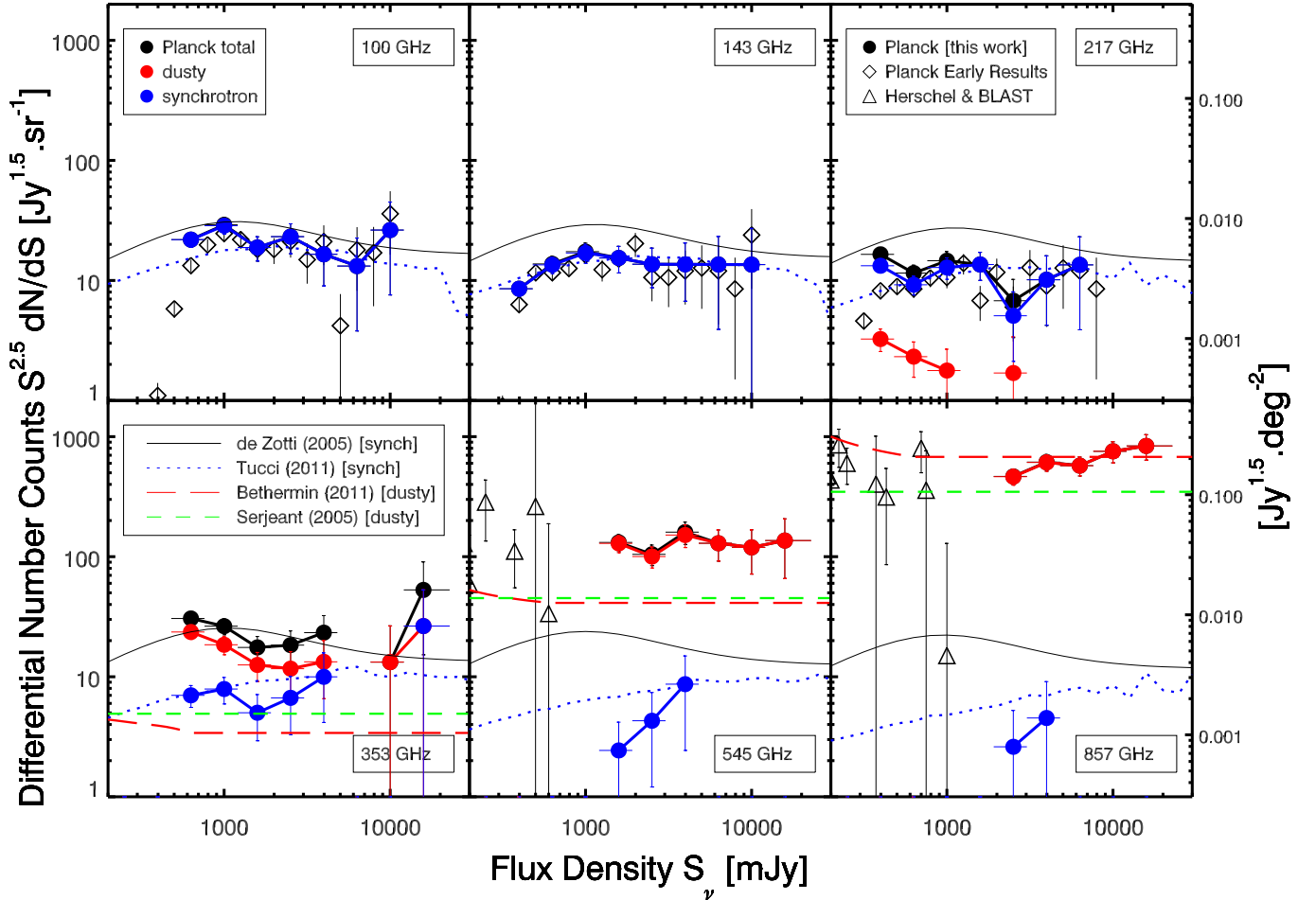


**Figure 9.** *Planck* differential number counts, normalised to the Euclidean value (i.e.  $S^{2.5}dN/dS$ ), compared with models and other data sets. *Planck* counts: total (black filled circles); dusty (red circles); synchrotron (blue circles). Four models are also plotted: [de Zotti et al. \(2005\)](#), dealing only with synchrotron sources – solid line); [Tucci et al. \(2011\)](#), dealing only with synchrotron sources – dots); [Bethermin et al. \(2011\)](#), dealing only with dusty sources – long dashes); [Serjeant & Harrison \(2005\)](#), dealing only with local dusty sources – short dashes). Other data sets: *Planck* early counts for 30 GHz-selected radio galaxies ([Planck Collaboration XIII, 2011](#)) at 100, 143 and 217 GHz (open diamonds); *Herschel* ATLAS and HerMES counts at 350 and 500  $\mu\text{m}$  from [Oliver et al. \(2010\)](#) and [Clements et al. \(2010\)](#); BLAST at the same two wavelengths, from [Bethermin et al. \(2010b\)](#), all shown as triangles. Left vertical axes are in units of  $\text{Jy}^{1.5} \text{sr}^{-1}$ , and the right vertical axis in  $\text{Jy}^{1.5} \text{deg}^{-2}$ .

### 5.3. *Planck* Number Counts and Models

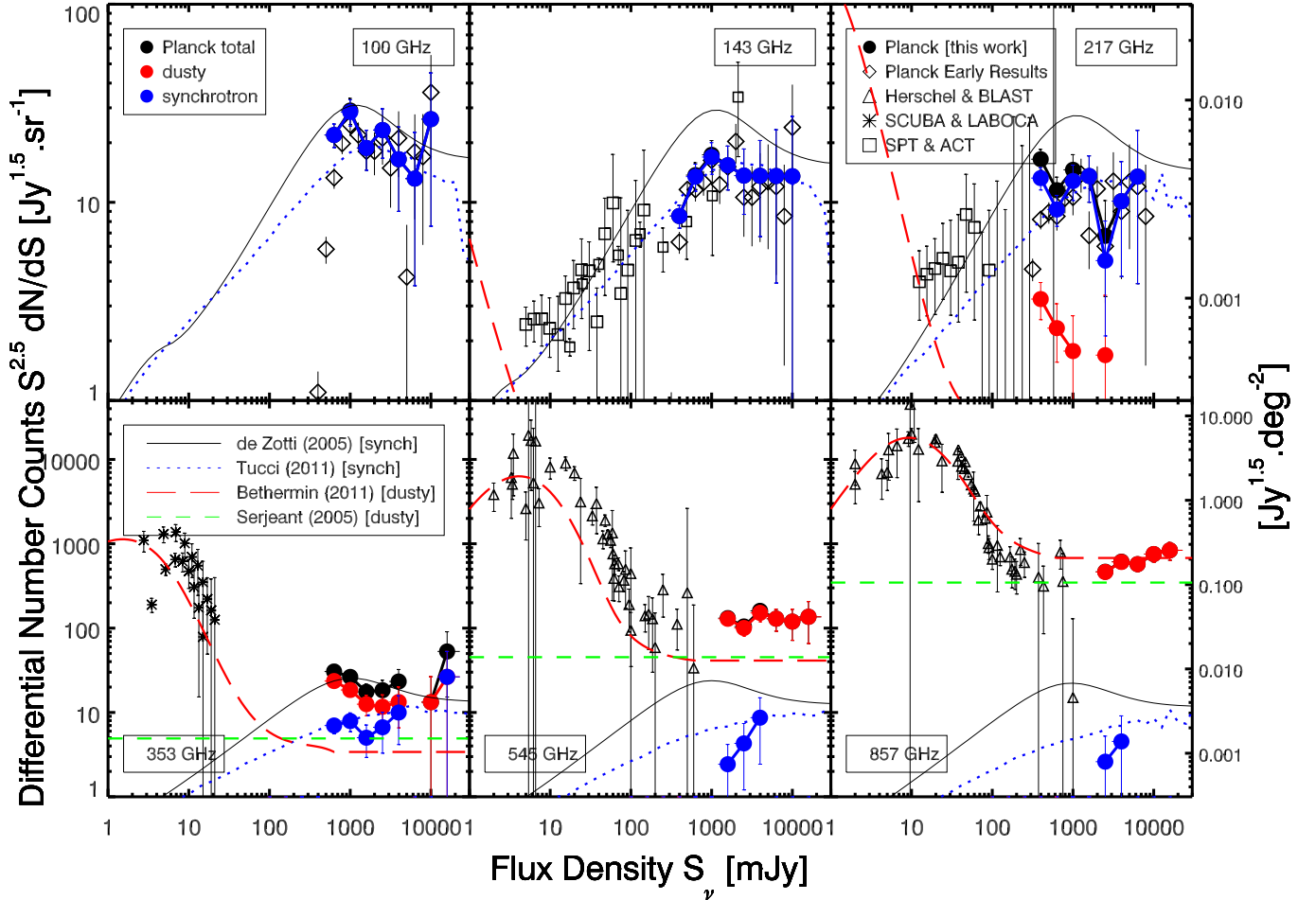
#### 5.3.1. Models

Fig. 9 and 10 display our present estimates of number counts of extragalactic point sources, based on ERCSC data, together with predictions from recent evolution models. These models focus either on radio-selected sources – i.e. sources with spectra dominated by synchrotron radiation at mm/submm wavelengths (“synchrotron sources”): [de Zotti et al. \(2005\)](#) and [Tucci et al. \(2011\)](#) – or on far-IR selected sources – i.e. sources with spectra dominated by thermal cold dust emission at mm/submm wavelengths (“dusty sources”): [Serjeant & Harrison \(2005\)](#) and [Bethermin et al. \(2011\)](#). Many other models exist in the literature, among which are [Le Borgne et al. \(2009\)](#), [Negrello et al. \(2009\)](#), [Pearson & Khan \(2009\)](#), [Rowan-Robinson \(2009\)](#), [Valiante et al. \(2009\)](#), [Franceschini et al. \(2010\)](#), [Lacey et al. \(2010\)](#), [Marsden et al. \(2011\)](#), [Wilman et al. \(2010\)](#), and [Rahmati & van Der Werf \(2011\)](#). A comparison is given with these models in Fig. 12 for 857 GHz.

The [de Zotti et al. \(2005\)](#) model focusses on radio sources, flat- and steep-spectrum, the latter having a component of dusty spheroidals and GPS (GHz peaked spectrum) sources. Its cosmological evolution for extragalactic radio sources is based on analysis of all the main source populations at GHz frequencies and currently provides a good fit to all data on number counts and on other statistics from  $\sim 5$  GHz and up to  $\sim 100$  GHz. This model adopts a simple power-law, with an almost “flat” spectral index ( $\alpha \approx -0.1$ ), for extrapolating the spectra of the brightest extragalactic sources (essentially “blazar”<sup>2</sup> sources) at frequencies above 100 GHz.

The [Tucci et al. \(2011\)](#) models provide a description of three populations of radio sources: steep-, flat-, and inverted-spectrum. The flat-spectrum population is further divided into Flat-Spectrum Radio Quasars (FSRQ), and BL Lacs. The main

<sup>2</sup> Blazars are jet-dominated extragalactic objects, observed within a small angle of the jet axis and characterized by a highly variable, non-thermal synchrotron emission at GHz frequencies in which the beamed component dominates the observed emission ([Angel & Stockman, 1980](#)).



**Figure 10.** Same as Fig. 9, but on a wider flux density scale and with the addition of ACT (Marriage et al., 2011) and SPT (Vieira et al., 2010) data as squares at 143 and 217 GHz, and SCUBA and LABOCA data as stars at 353 GHz (Borys et al., 2003; Coppin et al., 2006; Scott et al., 2006; Beelen et al., 2008; Weiss et al., 2009).

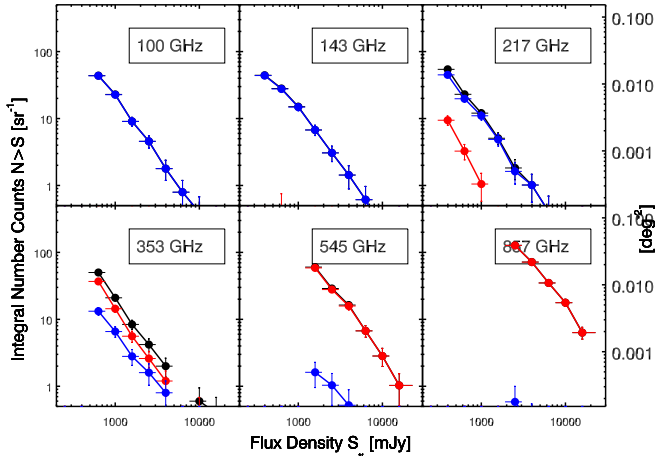


**Figure 11.** *Planck* integral number counts (filled circles); dusty (red); synchrotron (blue). Vertical axes are in number per steradian; right axis is in number per square degree. Counts are completeness-corrected. The same faint flux density cut as for differential counts is applied.

novelty of these models is the statistical prediction of the “break” frequency,  $\nu_M$ , in the spectra of blazar jets modeled by classi-

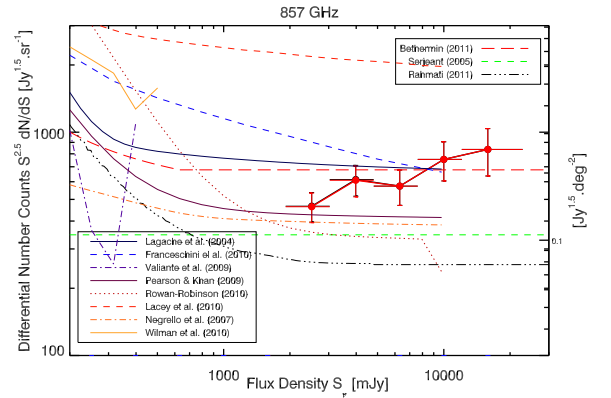


**Figure 12.** *Planck* differential number counts at 857 GHz, normalised to the Euclidean (i.e.  $S^{2.5} dN/dS$ ). *Planck* counts: total (black filled circles); dusty galaxies (red circles). Models: Betherrmin et al. (2011) (long red dashes – dusty); Serjeant & Harrison (2005) (short green dashes – dusty); Rahmati & van Der Werf (2011) (black dash-dot-dot-dot line). Other: Lagache et al. (2004); Negrello et al. (2007); Rowan-Robinson (2009); Valiante et al. (2009); Pearson & Khan (2009); Franceschini et al. (2010); Lacey et al. (2010); Wilman et al. (2010).

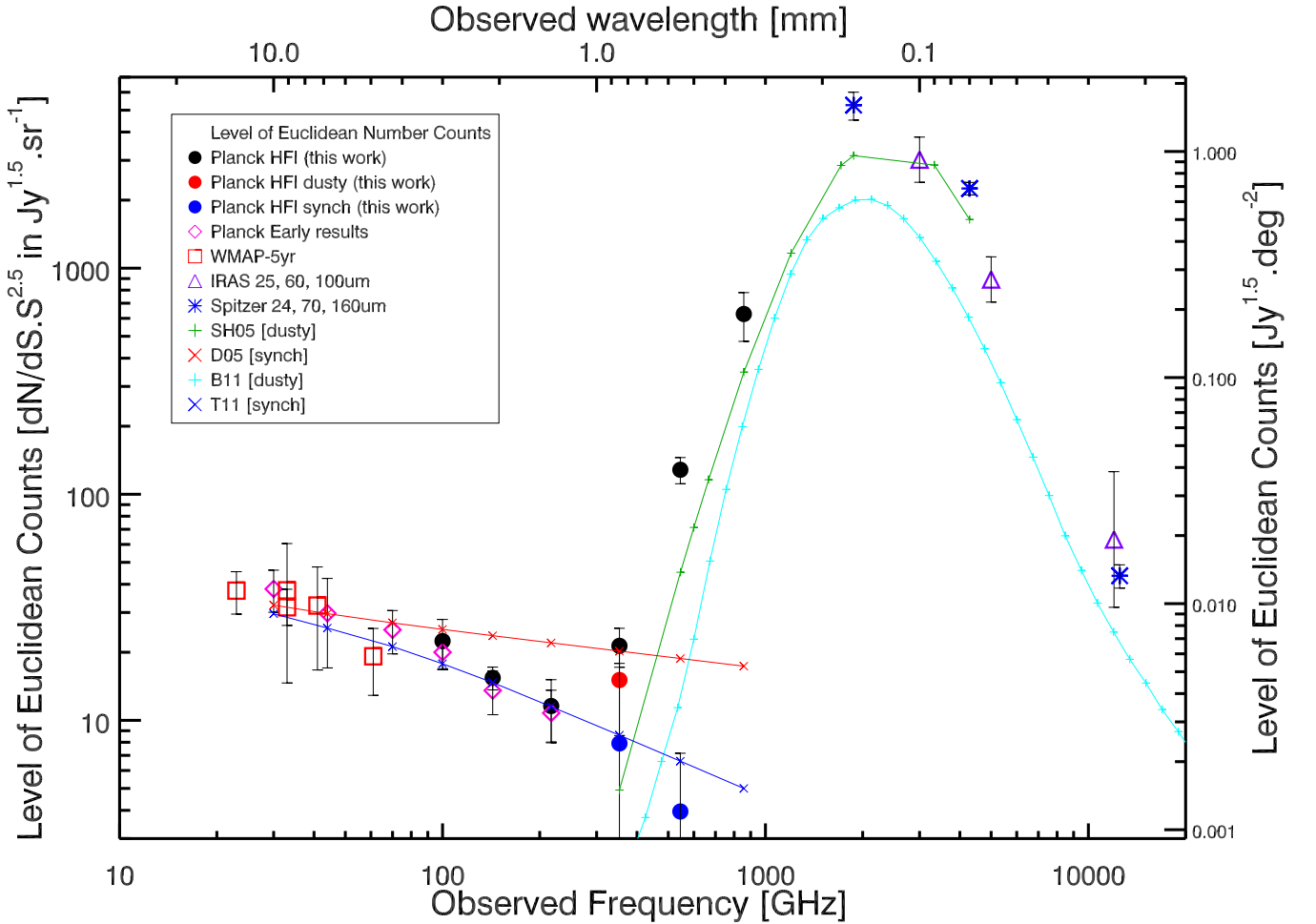


**Figure 13.** Euclidean level  $p$  (plateau in  $S^{2.5}dN/dS$ , see Eq. 1), expressed in number of galaxies times  $\text{Jy}^{1.5} \text{sr}^{-1}$  (or  $\text{Jy}^{1.5} \text{deg}^{-2}$  on the right axis) averaged between approximately 1 and 3 Jy at microwave to mid-IR frequencies. We specifically show: our *Planck* HFI results (black circles) – dusty source (red circles) and synchrotron sources (blue circles). The dusty 545 GHz point is almost on top of the total *Planck* point. *Planck* Early results (purple diamonds) from (Planck Collaboration XIII, 2011); *WMAP*-5year (red squares) from Wright et al. (2009); Massardi et al. (2009); de Zotti et al. (2010); *IRAS* 25, 60 and  $100\mu\text{m}$  results (purple triangles) from Hacking & Soifer (1991), Lonsdale & Hacking (1989), and Bertin & Dennefeld (1997); *Spitzer* 24, 70 and  $160\mu\text{m}$  (blue stars) from Bethermin et al. (2010a). We also plot the models (solid lines): Serjeant & Harrison (2005), based on *IRAS* and SCUBA data and dealing with dusty galaxies (SH05 green plus signs); Bethermin et al. (2011) (B11 light blue plus) dealing with dusty galaxies; de Zotti et al. (2005) (D05 red X) dealing with synchrotron sources; Tucci et al. (2011) (T11 blue X) for synchrotron sources. Values are given in Tab. 8.

cal, synchrotron-emission physics. The most successful of these models, “C2Ex”, assumes different distributions of break frequencies for BL Lac objects and Flat Spectrum Radio Quasars (FSRQs) – with the relevant synchrotron emission coming from more compact regions in the jets of the former objects. This model, developed to consistently fit the Atacama Cosmology Telescope (ACT) data (Marriage et al., 2011) at 148 GHz as well as the results published in the *Planck* Early paper Planck Collaboration XIII (2011) is able to give a very good fit to all published data on statistics of extragalactic radio sources: i.e. number counts and spectral index distributions. The model “C2Ex” also correctly predicts the number of blazars observed in the Herschel Astrophysical Terahertz Large Area Survey (H-ATLAS) at 600 GHz, as discussed in López-Caniego et al. (2012).

The Serjeant & Harrison (2005) model is based on the SED properties of local galaxies detected by *IRAS* and SCUBA in the SLUGS sample (Dunne et al., 2000). These local SEDs are used

in many models, including the Lapi et al. (2011) model (based on Lapi et al. 2006 and Granato et al. 2004) which links dark matter halo masses with the mass of black holes and the star formation rate.

Bethermin et al. (2011) present a backwards evolution model, taking into account IR galaxies, which is a parametric model fitting the fainter counts. It contains two families of SEDs: normal and starburst, from Lagache et al. (2004).

### 5.3.2. Synchrotron sources

The de Zotti et al. (2005) model over-predicts the number counts of extragalactic synchrotron sources detected by *Planck* at HFI frequencies. The main reason for this disagreement is the spectral steepening observed in ERCSC sources above about 70 GHz (Planck Collaboration XIII, 2011; Planck Collaboration XV, 2011), and already suggested by other data sets (González-Nuevo et al., 2008; Sadler et al., 2008).

The more recent model by [Tucci et al. \(2011\)](#) “C2Ex” is able to give a reasonable fit to the *Planck* number counts on bright extragalactic radio sources from 100 up to 545 GHz (and marginally at 857 GHz where our data are noisy). However, our current data at 100 and 217 GHz are consistently higher than the model number counts of synchrotron sources in the faintest flux density bin probed by ERCSC complete data (300 and 600 mJy, respectively). On the whole, the “C2Ex” model accounts well for the observed level of bright extragalactic radio sources up to 545 GHz.

### 5.3.3. Dusty sources

The [Serjeant & Harrison \(2005\)](#) model performs reasonably well at 857 GHz, but is lower than our observations at 545 and 353 GHz. The [Bethermin et al. \(2011\)](#) model has the same trend – it is compatible with the data at 857 GHz, but is lower than the observations by a factor of about 3 at 353 and 545 GHz. This is likely due to the limits of that model’s validity at high flux density (typically above one Jy). For both models, the likely origin of the discrepancy with our new, *Planck*, high-frequency data is the models’ inaccurate description of local SEDs. Since the counts of bright sources at high frequency mainly depend on the SED of low- $z$ , IR galaxies, rather than cosmological evolution at higher redshifts, any discrepancy with models is telling us more about their accuracy in reproducing the averaged SED of the low- $z$  Universe than about any cosmological evolution. This effect is also seen in the Euclidean level (Sect. 5.4 and Fig. 13).

### 5.3.4. Other models

Fig. 12 shows more models at 857 GHz. Most of the models do not explicitly include the counts at such high flux densities (and/or are subject to numerical uncertainties, like [Valiante et al. 2009](#); [Wilman et al. 2010](#)). We thus suggest that model predictions extend up to a few tens of Jy in order to provide a good anchor for the SEDs at low redshift. At 857 GHz, many models disagree with our data, e.g. [Negrello et al. \(2007\)](#), [Franceschini et al. \(2010\)](#), [Lacey et al. \(2010\)](#), [Rahmati & van Der Werf \(2011\)](#), [Rowan-Robinson et al. \(2010\)](#). Other models agree or marginally agree with our data, e.g. [Lagache et al. \(2004\)](#); [Pearson & Khan \(2009\)](#); [Bethermin et al. \(2011\)](#).

### 5.3.5. Main results

The two main results from the comparison with models are: 1) the good agreement of the [Tucci et al. \(2011\)](#) model with our counts of synchrotron-dominated sources, including for the first time at 353, 545 and marginally at 857 GHz; and 2) the failure of most models to reproduce the dusty-dominated sources between 353 and 857 GHz. This latter point is likely due to errors in the SEDs of local galaxies used (i.e. at redshifts less than 0.1 and flux densities larger than 1 Jy).

## 5.4. Beyond the number counts

### 5.4.1. *Planck* observations of the Euclidean level

The Euclidean level of the number counts, described as the plateau level,  $p$ , in the normalised differential number counts at high flux density,

$$dN/dS = p S^{-2.5} \quad (1)$$

mainly depends on the SED shape of galaxies (local galaxies in the case of high frequency observations).

Figure 13 shows  $p$  over more than two orders of magnitude in observed frequency, from the mid-IR to the radio range. The values of  $p$  are reported in Table 8. The Euclidean level was determined using number counts above 1 Jy (except for *Spitzer*, where number counts at fainter flux densities were used). Beyond our measurements at *Planck* HFI frequencies (total in black, but also by type: dusty and synchrotron), we also show the *Planck* early results at LFI and HFI 100 GHz frequencies ([Planck Collaboration XIII, 2011](#)), as well as *WMAP*-5year at Ka ([Wright et al., 2009](#)) and in all bands ([Massardi et al., 2009](#); [de Zotti et al., 2010](#)), and finally *IRAS* 25, 60 and 100  $\mu$ m results ([Lonsdale & Hacking, 1989](#); [Hacking & Soifer, 1991](#); [Bertin & Dennefeld, 1997](#)). The *Spitzer* level at 24, 70 and 160  $\mu$ m comes from counts above 8, 70 and 300 mJy, respectively ([Bethermin et al., 2010a](#)). We also plot the models of [Serjeant & Harrison \(2005\)](#) (based on *IRAS* and SCUBA 850  $\mu$ m local colors), of [de Zotti et al. \(2005\)](#), of [Bethermin et al. \(2011\)](#), and of [Tucci et al. \(2011\)](#).

At 100 GHz, our current and early *Planck* estimates are in good agreement. Also, the *Planck* LFI and *WMAP* estimates agree within the error bars. The *Planck* contribution is unique in disentangling the dusty from synchrotron sources in the key spectral regime around 300 GHz where the two populations contribute equally to the Euclidean level.

The *Planck* measurements of synchrotron sources between 30 and 217 GHz at LFI frequencies and lower HFI frequencies are very well reproduced by the [Tucci et al. \(2011\)](#) model “C2Ex”. The Euclidean level for synchrotron sources at 353 GHz is also well reproduced by this model.

The *Planck* measurements lie above the [Serjeant & Harrison \(2005\)](#) and [Bethermin et al. \(2011\)](#) models at the three upper HFI frequencies between 353 and 857 GHz. There are two explanations for this: (1) the presence of synchrotron galaxies in equal numbers to dusty galaxies between 217 and 353 GHz which are not seen in the *IRAS* 60  $\mu$ m selected sample; and (2) the cold dust component in the local Universe, although known for quite some time ([Stickel et al., 1998](#); [Dunne et al., 2000](#)), may have been underestimated (as *Planck* suggested, [Planck Collaboration XVI, 2011](#)) through a significant and largely unexplored cold ( $T < 20$  K) component in many nearby galaxies. This excess of submm emission is statistically confirmed here. At 545 GHz for instance, we measure  $p = (125 \pm 16) \text{ Jy}^{1.5} \text{ sr}^{-1}$  for the dusty galaxies; the [Serjeant & Harrison \(2005\)](#) model predicts  $45 \text{ Jy}^{1.5} \text{ sr}^{-1}$  (a factor of 2.7 lower) and the [Bethermin et al. \(2011\)](#) predicts  $10 \text{ Jy}^{1.5} \text{ sr}^{-1}$  (a factor of 12 lower). At 353 GHz, we measure  $p = 13 \pm 7 \text{ Jy}^{1.5} \text{ sr}^{-1}$  for the dusty galaxies, while the [Serjeant & Harrison \(2005\)](#) model predicts  $4.92 \text{ Jy}^{1.5} \text{ sr}^{-1}$  (a factor of 2.7 lower). This is in line with the cooler 60  $\mu$ m:450  $\mu$ m colour (i.e. smaller 60/450 flux ratio) found in the ERCSC ([Planck Collaboration XVI, 2011](#), e.g. their figure. 4) unlike those of the SLUGS sample ([Dunne et al., 2000](#)): *Planck* ERCSC sources can have a factor up to 10 smaller 60  $\mu$ m:450  $\mu$ m flux ratios.

### 5.4.2. Link between the Euclidean level for dusty galaxies and the local luminosity density

In the IR and submm, the bright counts of dusty galaxies probe only the local Universe, which can be approximated as a Euclidean space filled with non-evolving populations. The vol-



ume  $V_{\max}$  where a source with a luminosity density  $L_\nu$  is seen with a flux density larger than  $S_{\nu,\text{lim}}$  is:

$$V_{\max} = \frac{4\pi}{3} D_{\max}^3 = \frac{4\pi}{3} \left( \frac{L_\nu}{4\pi S_{\nu,\text{lim}}} \right)^{\frac{3}{2}}, \quad (2)$$

where  $D_{\max}$  is the maximum at distance at which a source can be detected, and  $S_{\nu,\text{lim}}$  the limiting flux density at frequency  $\nu$ . The contribution of sources with  $L_\nu - dL_\nu/2 < L_\nu < L_\nu + dL_\nu/2$  to the counts is then

$$\frac{dN(S_\nu > S_{\nu,\text{lim}})}{dL_\nu} = \frac{d^2N}{dL_\nu dV} \times \frac{L_\nu^{\frac{3}{2}}}{S_{\nu,\text{lim}}^{\frac{3}{2}} 6\sqrt{\pi}}, \quad (3)$$

where  $N(S_\nu > S_{\nu,\text{lim}})$  is the number of sources brighter than  $S_{\nu,\text{lim}}$  over the entire sky and  $\frac{d^2N}{dL_\nu dV}$  the local luminosity function. The integral counts  $dN(S_\nu > S_{\nu,\text{lim}})/d\Omega$  are linked to this local luminosity function by:

$$\frac{dN(S_\nu > S_{\nu,\text{lim}})}{d\Omega} = \frac{1}{4\pi} \int_{L_\nu=0}^{\infty} \frac{d^2N}{dL_\nu dV} \times \frac{L_\nu^{\frac{3}{2}}}{S_{\nu,\text{lim}}^{\frac{3}{2}} 6\sqrt{\pi}} dL_\nu \quad (4)$$

The differential counts  $d^2N/(dS_\nu d\Omega)$  are thus

$$\frac{d^2N}{dS_\nu d\Omega} = \frac{S_\nu^{-\frac{5}{2}}}{16\pi^{\frac{3}{2}}} \int_{L_\nu=0}^{\infty} \frac{d^2N}{dL_\nu dV} \times L_\nu^{\frac{3}{2}} dL_\nu \quad (5)$$

and the level  $p$  of the Euclidean plateau is thus

$$p_\nu = \frac{1}{16\pi^{\frac{3}{2}}} \int_{L_\nu=0}^{\infty} \frac{d^2N}{dL_\nu dV} \times L_\nu^{\frac{3}{2}} dL_\nu \quad (6)$$

The local monochromatic luminosity density  $\rho_\nu$  can be computed as

$$\rho_\nu = \int_{L_\nu=0}^{\infty} \frac{d^2N}{dL_\nu dV} \times L_\nu dL_\nu \quad (7)$$

If we assume a single mean color  $C$  between frequencies  $\nu_1$  and  $\nu_2$  (with  $S_{\nu_1} = CS_{\nu_2}$ ) for all the sources, we simply have the relation

$$\frac{\rho_{\nu_2}}{\rho_{\nu_1}} = C. \quad (8)$$

If we perform the same analysis on the level of the Euclidean plateau, we obtain

$$\frac{p_{\nu_2}}{p_{\nu_1}} = C^{\frac{3}{2}}. \quad (9)$$

The quantities  $p_\nu$  and  $\rho_\nu$  are thus linked by

$$\frac{\rho_{\nu_2}}{\rho_{\nu_1}} = \left( \frac{p_{\nu_2}}{p_{\nu_1}} \right)^{\frac{2}{3}} \quad (10)$$

We could use  $\rho_{60}$  (the *IRAS* local luminosity density at 60  $\mu\text{m}$ ) and  $p_{60}$  (the Euclidean level at 60  $\mu\text{m}$ ) as a reference, in order to derive  $\rho_\nu$ , the luminosity density of dusty galaxies at frequency  $\nu$  (with *IRAS* as a reference):

$$\rho_\nu = \left( \frac{p_\nu}{p_{60}} \right)^{\frac{2}{3}} \rho_{60} \quad (11)$$

However, the extrapolation of the dust emission from the FIR to the (sub-)millimetre wavelengths is uncertain (as our data

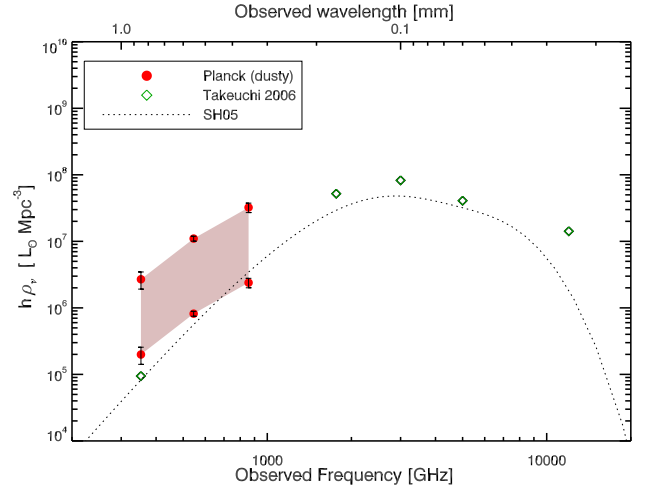


**Figure 14.** Monochromatic luminosity density  $\rho_\nu$  (in units of  $h L_\odot \text{Mpc}^{-3}$ ) of dusty galaxies, derived from the Euclidean level  $p$  and scaled to the luminosity density of: SCUBA 850  $\mu\text{m}$  data (Dunne et al., 2000; Serjeant & Harrison, 2005) (see Eq. 12); or *IRAS* 60  $\mu\text{m}$  data (Soifer & Neugebauer, 1991; Bertin & Dennefeld, 1997; Takeuchi et al., 2003) (see Eq. 11). Red circles: estimate from *Planck* for dusty galaxies (this work); green diamonds: compilation from Takeuchi et al. (2006); black dots: model from Serjeant & Harrison (2005). Values are given in Tab. 9. Our *Planck* estimates are in the shaded area.

show). We might instead want to use the luminosity density estimated at 850  $\mu\text{m}$  from previous studies, and correct them to account for the excess observed by *Planck*. We can thus use:

$$\rho_\nu = \left( \frac{p_\nu}{p_{850}} \right)^{\frac{2}{3}} \rho_{850} \quad (12)$$

Both the 60  $\mu\text{m}$ -based and the 850  $\mu\text{m}$ -based estimates are shown in Fig. 14 and discussed in the next section.

#### 5.4.3. Estimate of the local luminosity density for dusty galaxies

We use two reference wavelengths to derive  $\rho_\nu$ :

- at 60  $\mu\text{m}$  using *IRAS* data:  $\rho_{60}$  is estimated by Soifer & Neugebauer (1991) and Takeuchi et al. (2006);  $p_{60}$  by Soifer & Neugebauer (1991) and Bertin & Dennefeld (1997);
- at 850  $\mu\text{m}$  using SCUBA SLUGS:  $\rho_{850}$  is estimated by Dunne et al. (2000) and Takeuchi et al. (2006);  $p_{850}$  by Serjeant & Harrison (2005).

The values are:  $\rho_{60} = 4.08 \times 10^7 h L_\odot \text{Mpc}^{-3}$  and  $p_{60} = 891.3 \text{Jy}^{1.5} \text{sr}^{-1}$  at 60  $\mu\text{m}$ ;  $\rho_{850} = 9.45 \times 10^4 h L_\odot \text{Mpc}^{-3}$  and  $p_{850} = 4.92 \text{Jy}^{1.5} \text{sr}^{-1}$ . The use of two reference wavelengths is driven by the oversimplified hypothesis of a constant color  $C$  between two frequencies (assumptions described in Sect. 5.4.2). Computing  $\rho_\nu$  using two different reference wavelengths allows us to estimate the impact of this hypothesis.

The results of our estimated luminosity densities from this simple model are shown in Fig. 14: lower points using the SCUBA 850  $\mu\text{m}$  reference (Eq. 12); upper points using the *IRAS* 60  $\mu\text{m}$  reference (Eq. 11). The values are given in Tab. 9.

As expected, our *Planck* indirect upper estimate is higher than SLUGS at 353 GHz if we use 850  $\mu\text{m}$  as a reference. This is well in line with our value of  $p$  being 2.7 times higher, implying

a factor of 2 (i.e.  $2.7^{2/3}$ ) in the luminosity densities. On the other hand, our 353 GHz estimate using  $60\mu\text{m}$  as a reference falls way above the SCUBA estimate at  $850\mu\text{m}$ . This illustrates that caution is required when extrapolating FIR colors to the submm.

The true luminosity density should lie between our lower and upper estimates; the ratio equals 13.5. At 353 GHz, our estimate using SCUBA as a reference should be more relevant to use than the *IRAS* extrapolation.

## 6. Conclusion and Summary

From the *Planck* all-sky survey, we derive extragalactic number counts based on the ERCSC (Planck Collaboration VII, 2011) from 100 to 857 GHz (3 mm to  $350\mu\text{m}$ ). We use an 80 % completeness cut on three homogeneous zones, covering a total of about  $16000\text{ deg}^2$  ( $f_{\text{sky}} \sim 0.31$  to  $0.40$ ) outside a Galactic mask. We provide, for the first time, bright extragalactic counts at 353, 545 and 857 GHz (i.e., 850, 550 and  $350\mu\text{m}$ ; see Fig. 9). Our counts are in the Euclidean regime, and generally agree with other data sets, when available (Fig. 10).

Using multi-frequency information to classify the sources as dusty- or synchrotron-dominated (and measure their spectral indices), the most striking result is the contribution to the number counts by each population. The cross-over takes place at high frequencies, between 217 and 353 GHz, where both populations contribute almost equally to the number counts. At higher or lower frequencies, counts are quickly dominated by one or other population. We provide for the first time number counts estimates of synchrotron-dominated sources at high frequency (353 to 857 GHz) and dusty-dominated sources at lower frequencies (217 and 353 GHz).

Our counts provide new constraints on models which extend their predictions to bright flux densities. Existing models of synchrotron-dominated sources are not far off from our observations, with the model “C2Ex” of Tucci et al. (2011) performing particularly well at reproducing the synchrotron-dominated source counts up to 545 GHz (and marginally up to 857 GHz, where our statistics become sparse). Perhaps less expected is the failure of most models of dusty sources to reproduce all the high-frequency counts. The model of Bethermin et al. (2011) agrees marginally at 857 GHz but is too low at 545 GHz and at lower frequencies, while the model of Serjeant & Harrison (2005) is marginally lower at 857 GHz, fits the data well at 545 GHz, but is too low at 353 GHz. The likely origin of the discrepancies is an inaccurate description of the galaxy SEDs used at low redshift in these models. Indeed a cold dust component, seen e.g. by Planck Collaboration XVI (2011), is rarely included in the models at low redshift. This failure to reproduce high-frequency counts at bright flux density should not have any impact on the predictions at fainter flux densities and higher redshifts, as is shown in the good fit of *Herschel* counts. Nevertheless it tells us about the ubiquity of cold dust in the local Universe, at least in statistical terms.

Finally, in Fig. 13, we provide a review of the Euclidean plateau level  $p$  of the number counts, spanning nearly three orders of magnitude in both frequency and counts. The values of  $p$  are calculated for flux densities above 1 Jy, except in the case of *Spitzer* where fainter objects are used. Fig. 13 compares these results with some relevant models. The  $p$  value is usually not well reproduced by models (at least for de Zotti et al. 2005; Serjeant & Harrison 2005; Bethermin et al. 2011) in the synchrotron- or dust-dominated regimes. The Tucci et al. (2011) model, on the contrary, reproduces our observations of synchrotron sources, up to 545 GHz. This multifrequency diagnostic is a powerful tool

**Table 8.** Values of  $p$ , the Euclidean plateau level (in  $\text{Jy}^{1.5}\text{ sr}^{-1}$ ) from and *Planck* and other satellite data. The column “flag” indicates the nature of the sources (a=all; d=dusty; s=synch).

$\nu$ [GHz]	$p$ [ $\text{Jy}^{1.5}\text{ sr}^{-1}$ ]	Flag	Experiment	Reference
100	$22 \pm 5$	s	Planck	PlanckCollab2012
143	$15 \pm 1$	s	Planck	PlanckCollab2012
217	$11 \pm 3$	s	Planck	PlanckCollab2012
353	$21 \pm 4$	a	Planck	PlanckCollab2012
545	$128 \pm 17$	a	Planck	PlanckCollab2012
857	$627 \pm 152$	d	Planck	PlanckCollab2012
353	$15 \pm 6$	d	Planck	PlanckCollab2012
545	$125 \pm 15$	d	Planck	PlanckCollab2012
353	$7 \pm 9$	s	Planck	PlanckCollab2012
545	$3 \pm 3$	s	Planck	PlanckCollab2012
30	$38 \pm 8$	s	Planck	PlanckCollab2011
44	$29 \pm 12$	s	Planck	PlanckCollab2011
70	$25 \pm 5$	s	Planck	PlanckCollab2011
100	$20 \pm 3$	s	Planck	PlanckCollab2011
143	$13 \pm 2$	s	Planck	PlanckCollab2011
217	$10 \pm 2$	s	Planck	PlanckCollab2011
33	$31 \pm 1$	s	WMAP	Wright2009
23	$37 \pm 7$	s	WMAP	Massardi2009
33	$37 \pm 22$	s	WMAP	Massardi2009
41	$32 \pm 15$	s	WMAP	Massardi2009
61	$19 \pm 6$	s	WMAP	Massardi2009
12000	$63 \pm 1$	d	IRAS	Soifer91Bertin97
5000	$891 \pm 1$	d	IRAS	Soifer91Bertin97
3000	$3019 \pm 1$	d	IRAS	Soifer91Bertin97
12500	$43 \pm 5$	d	Spitzer	Bethermin2010
4285	$2252 \pm 143$	d	Spitzer	Bethermin2010
1875	$5261 \pm 743$	d	Spitzer	Bethermin2010

**Table 9.** Values of  $\rho_\nu$ , the luminosity density of dusty galaxies (in  $h\text{ L}_\odot\text{ Mpc}^{-3}$ ), inferred from the Euclidean plateau level  $p$  and scaled to the luminosity density at  $850\mu\text{m}$  (upper values) and  $60\mu\text{m}$  (lower values).

$\nu$ [GHz]	$\rho_\nu$ [scaled $850\mu\text{m}$ ] [ $h\text{ L}_\odot\text{ Mpc}^{-3}$ ]	$\rho_\nu$ [scaled $60\mu\text{m}$ ] [ $h\text{ L}_\odot\text{ Mpc}^{-3}$ ]
353	$(1.99 \pm 0.57) \times 10^5$	$(2.69 \pm 0.77) \times 10^6$
545	$(8.18 \pm 0.69) \times 10^5$	$(1.10 \pm 0.09) \times 10^7$
857	$(2.39 \pm 0.39) \times 10^6$	$(3.23 \pm 0.52) \times 10^7$

for investigating the SEDs of galaxies in the context of cosmological evolution – at relatively low redshifts for the dusty galaxies. We derive the local luminosity density range for dusty galaxies, based on simple considerations and using the SCUBA  $850\mu\text{m}$  and *IRAS*  $60\mu\text{m}$  luminosity density as a reference.

The *Planck* multi-frequency all-sky survey is very rich dataset, in particular for extragalactic studies. The final catalogue will be based on five sky surveys, while the present work is based on 1.6 surveys. With further data we expect to provide further constraints on the synchrotron vs. dusty dominated populations at all frequencies, and over a wider range in redshift.

**Acknowledgements.** Based on observations obtained with *Planck* (<http://www.esa.int/Planck>), an ESA science mission with instruments and contributions directly funded by ESA Member States, NASA, and Canada.

The development of *Planck* has been supported by: ESA; CNES and CNRS/INSU-IN2P3-INP (France); ASI, CNR, and INAF (Italy); NASA and DoE (USA); STFC and UKSA (UK); CSIC, MICINN and JA (Spain); Tekes, AoF and CSC (Finland); DLR and MPG (Germany); CSA (Canada); DTU Space (Denmark); SER/SSO (Switzerland); RCN (Norway); SFI (Ireland); FCT/MCTES (Portugal); and PRACE (EU). This research has made use of the

SIMBAD database, operated at CDS, Strasbourg, France. This research has made use of the NASA/IPAC Extragalactic Database (NED) which is operated by the Jet Propulsion Laboratory, California Institute of Technology, under contract with the National Aeronautics and Space Administration. This research has made use of the NASA/ IPAC Infrared Science Archive, which is operated by the Jet Propulsion Laboratory, California Institute of Technology, under contract with the National Aeronautics and Space Administration. This publication makes use of data products from the Wide-field Infrared Survey Explorer, which is a joint project of the University of California, Los Angeles, and the Jet Propulsion Laboratory/California Institute of Technology, funded by the National Aeronautics and Space Administration.

## References

- Angel, J. R. P. & Stockman, H. S. 1980, *ARA&A*, 18:321–361.
- Ashby, M. L. N., Hacking, P. B., Houck, J. R., Soifer, B. T., & Weisstein, E. W. 1996, *ApJ*, 456:428.
- Barger, A. J., Cowie, L. L., & Sanders, D. B. 1999, *ApJ*, 518:L5.
- Beelen, A., Omont, A., Bavouzet, N., Kovacs, A. 2008, *A&A*, 485, 645.
- Bennett, C. L., Halpern, M., Hinshaw, G., Jarosik, N., Kogut, A., Limon, M., Meyer, S. S., Page, L., Spergel, D. N., Tucker, G. S., Wollack, E., Wright, E. L., Barnes, C., Greason, M. R., Hill, R. S., Komatsu, E., Nolte, M. R., Odegard, N., Peiris, H. V., Verde, L., & Weiland, J. L. 2003, *Astrophys. J. Suppl. Ser.*, 148:1.
- Bersanelli, M., Mandolesi, N., Butler, R. C., Mennella, A., Villa, F. et al. September 2010, *A&A*, 520:A4.
- Bertin, E. & Dennefeld, M. 1997, *A&A*, 317:43.
- Bethermin, M., Dole, H., Beelen, A., & Aussel, H. 2010a, *A&A*, 512:A78.
- Bethermin, M., Dole, H., Cousin, M., & Bavouzet, N. 2010b, *A&A*, 516:A43.
- Bethermin, M., Dole, H., Lagache, G., Le Borgne, D., & Penin, A. 2011, *A&A*, 529:A4.
- Blain, A. W., Kneib, J. P., Ivison, R. J., & Smail, I. 1999, *ApJ*, 512:L87.
- Boggess, N. W., Mather, J. C., Weiss, R., Bennett, C. L., Cheng, E. S., et al. 1992, *ApJ*, 397:420.
- C. Borys, S. Chapman; M. Halpern; D. Scott, 2003, *MNRAS*, 344, 385.
- Clements, D. L., Rigby, E., Maddox, S., Dunne, L., Mortier, A., et al. arXiv:1005.2409, 2010.
- Coppin, K., Chapin, E. L., Mortier, A. M. J., Scott, S. E., Borys, C., et al. 2006, *MNRAS*, 372:1621–1652.
- de Zotti, G., Ricci, R., Mesa, D., Silva, L., Mazzotta, P., Toffolatti, L., & González-Nuevo, J. 2005, *A&A*, 431:893–903.
- de Zotti, G., Massardi, M., Negrello, M., & Wall, J. 2010, *Astronomy and Astrophysics Review*, 18:1–65.
- Delabrouille, J. et al. 2012, *A&A*, submitted, arXiv:1207.3675.
- Dole, H., Gispert, R., Lagache, G., Puget, J. L., Bouchet, F. R., et al. 2001, *A&A*, 372:364.
- Dole, H., Floc'h, E. L., Perez-Gonzalez, P. G., Papovich, C., Egami, E., et al. 2004, *Astrophys. J. Suppl. Ser.*, 154:87.
- Dunne, L., Eales, S., Edmunds, M., Ivison, R., Alexander, P., & Clements, D. L. 2000, *MNRAS*, 315:115.
- Franceschini, A., Rodighiero, G., Vaccari, M., Berta, S., Marchetti, L., & Mainetti, G. 2010, *A&A*, 517:74.
- Frayser, D. T., Fadda, D., Yan, L., Marleau, F. R., Choi, P. I., et al. 2006, *AJ*, 131:250.
- Genzel, R. & Cesarsky, C. J. 2000, *ARA&A*, 38:761.
- Gold, B., Odegard, N., Weiland, J. L., Hill, R. S., Kogut, A., et al. 2011, *Astrophys. J. Suppl. Ser.*, 192:15.
- González-Nuevo, J., Massardi, M., Argüeso, F., Herranz, D., Toffolatti, L., Sanz, J. L., López-Caniego, M., & de Zotti, G. 2008, *MNRAS*, 384:711–718.
- Górski, K. M., Hivon, E., Banday, A. J., Wandelt, B. D., Hansen, F. K., Reinecke, M., & Bartelmann, M. April 2005, *ApJ*, 622:759–771.
- Granato, G. L., de Zotti, G., Silva, L., Bressan, A., & Danese, L. 2004, *ApJ*, 600:580.
- Greve, T. R., Ivison, R. J., Bertoldi, F., Stevens, J. A., Dunlop, J. S., Lutz, D., & Carilli, C. L. 2004, *MNRAS*, 354:779–797.
- Hacking, P. B. & Soifer, B. T. 1991, *ApJ*, 367:L49.
- Herranz D. et al. 2012, *A&A*, submitted, arXiv:1204.3917
- Ivison, R. J., Smail, I., Barger, A. J., Kneib, J. P., Blain, A. W., Owen, F. N., Kerr, T. H., & Cowie, L. L. 2000, *MNRAS*, 315:209.
- Jarosik, N., Bennett, C. L., Dunkley, J., Gold, B., Greason, M. R., et al. 2011, *Astrophys. J. Suppl. Ser.*, 192:14.
- Lacey, C. G., Baugh, C. M., Frenk, C. S., Benson, A. J., Orsi, A., Silva, L., Granato, G. L., & Bressan, A. 2010, *MNRAS*, 405:2–28.
- Lagache, G., Dole, H., Puget, J. L., Perez-Gonzalez, P. G., Floc'h, E. L., et al. 2004, *Astrophys. J. Suppl. Ser.*, 154:112.
- Lamarre, J., Puget, J., Ade, P. A. R., Bouchet, F., Guyot, G., et al. 2010, *A&A*, 520:A9.
- Lapi, A., Shankar, F., Mao, J., Granato, G. L., Silva, L., de Zotti, G., & Danese, L. 2006, *ApJ*, 650:42.
- Lapi, A., Gonzalez-Nuevo, J., Fan, L., Bressan, A., de Zotti, G., et al. Herschel-atlas galaxy counts and high redshift luminosity functions: The formation of massive early type galaxies. arXiv:1108.3911, 2011.
- Larson, D., Dunkley, J., Hinshaw, G., Komatsu, E., Nolte, M. R., et al. 2011, *Astrophys. J. Suppl. Ser.*, 192:16.
- Le Borgne, D., Elbaz, D., Ocirk, P., & Pichon, C. 2009, *A&A*, 504:727–740.
- Leahy, J. P., Bersanelli, M., D’Arcangelo, O., Ganga, K., Leach, S. M., et al. September 2010, *A&A*, 520:A8.
- Lonsdale, C. J. & Hacking, P. B. 1989, *ApJ*, 339:712.
- López-Caniego et al. 2012; arXiv:1205.1929.
- Mandolesi, N., Bersanelli, M., Butler, R. C., Artal, E., Baccigalupi, C., et al. September 2010, *A&A*, 520:A3.
- Marriage et al. 2011, *ApJ*, 731, 100.
- Marsden, G., Chapin, E. L., Halpern, M., Patanchon, G., Scott, D., Truch, M. D. P., Valiante, E., Viero, M. P., & Wiebe, D. V. 2011, *MNRAS*, 417:1192–1209.
- Massardi, M., Lopez-Caniego, M., González-Nuevo, J., Herranz, D., de Zotti, G., & Sanz, J. L. 2009, *MNRAS*, 392:733–742.
- Mennella et al. 2011, *A&A*, 536:A3.
- Murakami, H., Baba, H., Barthel, P., Clements, D. L., Cohen, M., et al. 2007, *Publications of the Astronomical Society of Japan*, 59:369.
- Murdoch, H. S., Crawford, D. F., Jauncey, D. L., 1973, *ApJ*, 183, 1.
- Negrello, M., Perrotta, F., González-Nuevo, J., Silva, L., de Zotti, G., Granato, G. L., Baccigalupi, C., & Danese, L. 2007, *MNRAS*, 377:1557–1568.
- Negrello, M., Serjeant, S., Pearson, C., Takagi, T., Efstathiou, A., et al. 2009, *MNRAS*, 394:375–397.
- Neugebauer, G., Habing, H. J., van Duinen, R., Aumann, H. H., Baud, B., et al. 1984, *ApJ*, 278:L1.
- Oliver, S. J., Wang, L., Smith, A. J., Altieri, B., Amblard, A., et al. arXiv:1005.2184, 2010.
- Patanchon, G., Ade, P. A. R., Bock, J. J., Chapin, E. L., Devlin, M. J., et al. 2009, *ApJ*, 707:1750.
- Pearson, C. & Khan, S. A. 2009, *MNRAS*, 399:L11–L15.
- Peel, M. W., Dickinson, C., Davies, R. D., Clements, D. L., & Beswick, R. J. 2011, *MNRAS*, 416:L99–L103.
- Planck Collaboration I. 2011, *A&A*, 536:A1.
- Planck Collaboration II. 2011, *A&A*, 536:A2.
- Planck Collaboration VII. 2011, *A&A*, 536:A7.
- Planck Collaboration XIII. 2011, *A&A*, 536:A13.
- Planck Collaboration XIV. 2011, *A&A*, 536:A14.
- Planck Collaboration XV. 2011, *A&A*, 536:A15.
- Planck Collaboration XVI. 2011, *A&A*, 536:A16.
- Planck Collaboration XXIII. 2011, *A&A*, 536:A23.
- Planck Collaboration. 2011, *The Explanatory Supplement to the Planck Early Release Compact Source Catalogue*. ESA.
- Planck HFI Core Team. 2011a, *A&A*, 536:A4.
- Planck HFI Core Team. 2011b, *A&A*, 536:A6.
- Rahmati, A. & van Der Werf, P. P. 2011, *MNRAS*, 418:176–194.
- Rosset, C., Tristram, M., Ponthieu, N., Ade, P., Aumont, J., et al. September 2010, *A&A*, 520:A13.
- Rowan-Robinson, M., Broadhurst, T., Oliver, S. J., Taylor, A. N., Lawrence, A., et al. 1991, *Nature*, 351:719.
- Rowan-Robinson, M., Roseboom, I. G., Vaccari, M., Amblard, A., Arumugam, et al. 2010, *MNRAS*, 409:2–11.
- Rowan-Robinson, M. 2009, *MNRAS*, 394:117–123.
- Sadler, E. M., Ricci, R., Ekers, R. D., Sault, R. J., Jackson, C. A., & de Zotti, G. 2008, *MNRAS*, 385:1656–1672.
- Scott S. E., Dunlop J., Serjeant S. 2006, *MNRAS*, 370, 1057
- Serjeant, S. & Harrison, D. 2005, *MNRAS*, 356:192–204.
- Soifer, B. T. & Neugebauer, G. 1991, *AJ*, 101:354.
- Soifer, B. T., Helou, G., & Werner, M. 2008, *ARA&A*, 46:201–240.
- Stickel, M., Bogun, S., Lemke, D., Klaas, U., Toth, L. V., et al. 1998, *A&A*, 336:116.
- Takeuchi, T. T., Yoshikawa, K., & Ishii, T. T. 2003, *ApJ*, 587:L89.
- Takeuchi, T. T., Ishii, T. T., Dole, H., Dennefeld, M., Lagache, G., & Puget, J. L. 2006, *A&A*, 448:525.
- Tauber, J. A., Mandolesi, N., Puget, J., Banos, T., Bersanelli, M., et al. September 2010, *A&A*, 520:A1.
- Tucci, M., Toffolatti, L., de Zotti, G., & Martínez-González, E. 2011, *A&A*, 533:A57.
- Valiante, E., Lutz, D., Sturm, E., Genzel, R., & Chapin, E. L. 2009, *ApJ*, 701:1814.
- Vernstrom, T., Scott, D., & Wall, J. V. 2011, *MNRAS*, 415:3641–3648.
- Vieira, J. D., Crawford, T. M., Switzer, E. R., Ade, P. A. R., Aird, et al. 2010, *ApJ*, 719:763.
- Weiss, A., Ivison, R. J., Downes, D., Walter, F., Cirasuolo, M., & Menten, K. M. 2009, *ApJ*, 705:L45–L47.
- Wilman, R. J., Jarvis, M. J., Mauch, T., Rawlings, S., & Hickey, S. 2010, *MNRAS*, 405:447–461.
- Wright, E. L., Chen, X., Odegard, N., Bennett, C. L., Hill, R. S., et al. February 2009, *ApJS*, 180:283–295.



Wright, E. L., Eisenhardt, P. R. M., Mainzer, A. K., Ressler, M. E., Cutri, R. M et al. 2010, *AJ*, 140:1868.  
 Zacchei et al. 2011, *A&A*, 536:A5.

<sup>1</sup> APC, AstroParticule et Cosmologie, Université Paris Diderot, CNRS/IN2P3, CEA/Irfu, Observatoire de Paris, Sorbonne Paris Cité, 10, rue Alice Domon et Léonie Duquet, 75205 Paris Cedex 13, France

<sup>2</sup> Aalto University Metsähovi Radio Observatory, Metsähovintie 114, FIN-02540 Kylmäla, Finland

<sup>3</sup> Agenzia Spaziale Italiana Science Data Center, c/o ESRIN, via Galileo Galilei, Frascati, Italy

<sup>4</sup> Agenzia Spaziale Italiana, Viale Liegi 26, Roma, Italy

<sup>5</sup> Astrophysics Group, Cavendish Laboratory, University of Cambridge, J J Thomson Avenue, Cambridge CB3 0HE, U.K.

<sup>6</sup> Atacama Large Millimeter/submillimeter Array, ALMA Santiago Central Offices, Alonso de Cordova 3107, Vitacura, Casilla 763 0355, Santiago, Chile

<sup>7</sup> CITA, University of Toronto, 60 St. George St., Toronto, ON M5S 3H8, Canada

<sup>8</sup> CNRS, IRAP, 9 Av. colonel Roche, BP 44346, F-31028 Toulouse cedex 4, France

<sup>9</sup> California Institute of Technology, Pasadena, California, U.S.A.

<sup>10</sup> Centre of Mathematics for Applications, University of Oslo, Blindern, Oslo, Norway

<sup>11</sup> Centro de Estudios de Física del Cosmos de Aragón (CEFCA), Plaza San Juan, 1, planta 2, E-44001, Teruel, Spain

<sup>12</sup> Computational Cosmology Center, Lawrence Berkeley National Laboratory, Berkeley, California, U.S.A.

<sup>13</sup> Consejo Superior de Investigaciones Científicas (CSIC), Madrid, Spain

<sup>14</sup> DSM/Irfu/SPP, CEA-Saclay, F-91191 Gif-sur-Yvette Cedex, France

<sup>15</sup> DTU Space, National Space Institute, Juliane Mariesvej 30, Copenhagen, Denmark

<sup>16</sup> Département de Physique Théorique, Université de Genève, 24, Quai E. Ansermet, 1211 Genève 4, Switzerland

<sup>17</sup> Departamento de Física Fundamental, Facultad de Ciencias, Universidad de Salamanca, 37008 Salamanca, Spain

<sup>18</sup> Departamento de Física, Universidad de Oviedo, Avda. Calvo Sotelo s/n, Oviedo, Spain

<sup>19</sup> Departamento de Matemáticas, Universidad de Oviedo, Avda. Calvo Sotelo s/n, Oviedo, Spain

<sup>20</sup> Department of Astrophysics, IMAPP, Radboud University, P.O. Box 9010, 6500 GL Nijmegen, The Netherlands

<sup>21</sup> Department of Physics & Astronomy, University of British Columbia, 6224 Agricultural Road, Vancouver, British Columbia, Canada

<sup>22</sup> Department of Physics and Astronomy, Dana and David Dornsife College of Letter, Arts and Sciences, University of Southern California, Los Angeles, CA 90089, U.S.A.

<sup>23</sup> Department of Physics and Astronomy, Tufts University, Medford, MA 02155, U.S.A.

<sup>24</sup> Department of Physics, Gustaf Hållströmin katu 2a, University of Helsinki, Helsinki, Finland

<sup>25</sup> Department of Physics, Princeton University, Princeton, New Jersey, U.S.A.

<sup>26</sup> Department of Physics, University of California, Berkeley, California, U.S.A.

<sup>27</sup> Department of Physics, University of California, One Shields Avenue, Davis, California, U.S.A.

<sup>28</sup> Department of Physics, University of California, Santa Barbara, California, U.S.A.

<sup>29</sup> Department of Physics, University of Illinois at Urbana-Champaign, 1110 West Green Street, Urbana, Illinois, U.S.A.

<sup>30</sup> Department of Statistics, Purdue University, 250 N. University Street, West Lafayette, Indiana, U.S.A.

<sup>31</sup> Dipartimento di Fisica e Astronomia G. Galilei, Università degli Studi di Padova, via Marzolo 8, 35131 Padova, Italy

<sup>32</sup> Dipartimento di Fisica, Università La Sapienza, P. le A. Moro 2, Roma, Italy

<sup>33</sup> Dipartimento di Fisica, Università degli Studi di Milano, Via Celoria, 16, Milano, Italy

<sup>34</sup> Dipartimento di Fisica, Università degli Studi di Trieste, via A. Valerio 2, Trieste, Italy

<sup>35</sup> Dipartimento di Fisica, Università di Ferrara, Via Saragat 1, 44122 Ferrara, Italy

<sup>36</sup> Dipartimento di Fisica, Università di Roma Tor Vergata, Via della Ricerca Scientifica, 1, Roma, Italy

<sup>37</sup> Dipartimento di Matematica, Università di Roma Tor Vergata, Via della Ricerca Scientifica, 1, Roma, Italy

<sup>38</sup> Discovery Center, Niels Bohr Institute, Blegdamsvej 17, Copenhagen, Denmark

<sup>39</sup> Dpto. Astrofísica, Universidad de La Laguna (ULL), E-38206 La Laguna, Tenerife, Spain

<sup>40</sup> European Southern Observatory, ESO Vitacura, Alonso de Cordova 3107, Vitacura, Casilla 19001, Santiago, Chile

<sup>41</sup> European Space Agency, ESAC, Planck Science Office, Camino bajo del Castillo, s/n, Urbanización Villafranca del Castillo, Villanueva de la Cañada, Madrid, Spain

<sup>42</sup> European Space Agency, ESTEC, Keplerlaan 1, 2201 AZ Noordwijk, The Netherlands

<sup>43</sup> Haverford College Astronomy Department, 370 Lancaster Avenue, Haverford, Pennsylvania, U.S.A.

<sup>44</sup> Helsinki Institute of Physics, Gustaf Hållströmin katu 2, University of Helsinki, Helsinki, Finland



- <sup>45</sup> INAF - Osservatorio Astronomico di Padova, Vicolo dell'Osservatorio 5, Padova, Italy
- <sup>46</sup> INAF - Osservatorio Astronomico di Roma, via di Frascati 33, Monte Porzio Catone, Italy
- <sup>47</sup> INAF - Osservatorio Astronomico di Trieste, Via G.B. Tiepolo 11, Trieste, Italy
- <sup>48</sup> INAF Istituto di Radioastronomia, Via P. Gobetti 101, 40129 Bologna, Italy
- <sup>49</sup> INAF/IASF Bologna, Via Gobetti 101, Bologna, Italy
- <sup>50</sup> INAF/IASF Milano, Via E. Bassini 15, Milano, Italy
- <sup>51</sup> INFN, Sezione di Roma 1, Università di Roma Sapienza, Piazzale Aldo Moro 2, 00185, Roma, Italy
- <sup>52</sup> IPAG: Institut de Planétologie et d'Astrophysique de Grenoble, Université Joseph Fourier, Grenoble 1 / CNRS-INSU, UMR 5274, Grenoble, F-38041, France
- <sup>53</sup> ISDC Data Centre for Astrophysics, University of Geneva, ch. d'Ecogia 16, Versoix, Switzerland
- <sup>54</sup> IUCAA, Post Bag 4, Ganeshkhind, Pune University Campus, Pune 411 007, India
- <sup>55</sup> Imperial College London, Astrophysics group, Blackett Laboratory, Prince Consort Road, London, SW7 2AZ, U.K.
- <sup>56</sup> Infrared Processing and Analysis Center, California Institute of Technology, Pasadena, CA 91125, U.S.A.
- <sup>57</sup> Institut Néel, CNRS, Université Joseph Fourier Grenoble I, 25 rue des Martyrs, Grenoble, France
- <sup>58</sup> Institut Universitaire de France, 103, bd Saint-Michel, 75005, Paris, France
- <sup>59</sup> Institut d'Astrophysique Spatiale, CNRS (UMR8617) Université Paris-Sud 11, Bâtiment 121, Orsay, France
- <sup>60</sup> Institut d'Astrophysique de Paris, CNRS (UMR7095), 98 bis Boulevard Arago, F-75014, Paris, France
- <sup>61</sup> Institut de Ciències de l'Espai, CSIC/IEEC, Facultat de Ciències, Campus UAB, Torre C5 par-2, Bellaterra 08193, Spain
- <sup>62</sup> Institute for Space Sciences, Bucharest-Magurale, Romania
- <sup>63</sup> Institute of Astronomy and Astrophysics, Academia Sinica, Taipei, Taiwan
- <sup>64</sup> Institute of Astronomy, University of Cambridge, Madingley Road, Cambridge CB3 0HA, U.K.
- <sup>65</sup> Institute of Theoretical Astrophysics, University of Oslo, Blindern, Oslo, Norway
- <sup>66</sup> Instituto de Astrofísica de Canarias, C/Vía Láctea s/n, La Laguna, Tenerife, Spain
- <sup>67</sup> Instituto de Física de Cantabria (CSIC-Universidad de Cantabria), Avda. de los Castros s/n, Santander, Spain
- <sup>68</sup> Jet Propulsion Laboratory, California Institute of Technology, 4800 Oak Grove Drive, Pasadena, California, U.S.A.
- <sup>69</sup> Jodrell Bank Centre for Astrophysics, Alan Turing Building, School of Physics and Astronomy, The University of Manchester, Oxford Road, Manchester, M13 9PL, U.K.
- <sup>70</sup> Kavli Institute for Cosmology Cambridge, Madingley Road, Cambridge, CB3 0HA, U.K.
- <sup>71</sup> LAL, Université Paris-Sud, CNRS/IN2P3, Orsay, France
- <sup>72</sup> LERMA, CNRS, Observatoire de Paris, 61 Avenue de l'Observatoire, Paris, France
- <sup>73</sup> Laboratoire AIM, IRFU/Service d'Astrophysique - CEA/DSM - CNRS - Université Paris Diderot, Bât. 709, CEA-Saclay, F-91191 Gif-sur-Yvette Cedex, France
- <sup>74</sup> Laboratoire Traitement et Communication de l'Information, CNRS (UMR 5141) and Télécom ParisTech, 46 rue Barrault F-75634 Paris Cedex 13, France
- <sup>75</sup> Laboratoire de Physique Subatomique et de Cosmologie, Université Joseph Fourier Grenoble I, CNRS/IN2P3, Institut National Polytechnique de Grenoble, 53 rue des Martyrs, 38026 Grenoble cedex, France
- <sup>76</sup> Laboratoire de Physique Théorique, Université Paris-Sud 11 & CNRS, Bâtiment 210, 91405 Orsay, France
- <sup>77</sup> Lawrence Berkeley National Laboratory, Berkeley, California, U.S.A.
- <sup>78</sup> Max-Planck-Institut für Astrophysik, Karl-Schwarzschild-Str. 1, 85741 Garching, Germany
- <sup>79</sup> National University of Ireland, Department of Experimental Physics, Maynooth, Co. Kildare, Ireland
- <sup>80</sup> Niels Bohr Institute, Blegdamsvej 17, Copenhagen, Denmark
- <sup>81</sup> Observational Cosmology, Mail Stop 367-17, California Institute of Technology, Pasadena, CA, 91125, U.S.A.
- <sup>82</sup> Optical Science Laboratory, University College London, Gower Street, London, U.K.
- <sup>83</sup> SISSA, Astrophysics Sector, via Bonomea 265, 34136, Trieste, Italy
- <sup>84</sup> School of Physics and Astronomy, Cardiff University, Queens Buildings, The Parade, Cardiff, CF24 3AA, U.K.
- <sup>85</sup> Space Sciences Laboratory, University of California, Berkeley, California, U.S.A.
- <sup>86</sup> Stanford University, Dept of Physics, Varian Physics Bldg, 382 Via Pueblo Mall, Stanford, California, U.S.A.
- <sup>87</sup> UPMC Univ Paris 06, UMR7095, 98 bis Boulevard Arago, F-75014, Paris, France
- <sup>88</sup> Université de Toulouse, UPS-OMP, IRAP, F-31028 Toulouse cedex 4, France
- <sup>89</sup> Universities Space Research Association, Stratospheric Observatory for Infrared Astronomy, MS 211-3, Moffett Field, CA 94035, U.S.A.
- <sup>90</sup> University of Granada, Departamento de Física Teórica y del Cosmos, Facultad de Ciencias, Granada, Spain

<sup>91</sup> Warsaw University Observatory, Aleje Ujazdowskie 4, 00-478 Warszawa, Poland

## Appendix A: Spectral classification; effect of intermediate sources and photometric noise

In this appendix, we investigate the fate of the so-called “intermediate” sources, i.e. the sources defined as such in Sect. 3.

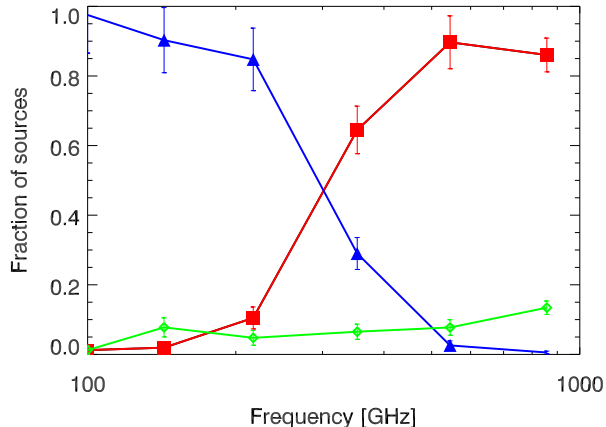


**Figure A.1.** Like Fig. 8, the fraction of source type (dusty, red squares; synch, blue triangles) as a function of frequency (sample cut at 80 % completeness, used for number counts). The difference is that we have now included the “intermediate” population (green diamonds). We can see that at most 13 % of our classification as dusty or synchrotron can be affected by intermediate sources. Our number counts by type (above 80 % completeness) are thus almost unaffected by these intermediate type sources.

Fig. A.1 shows the fraction of sources (like Fig. 8) by type (dusty, synchrotron, and now intermediate) as a function of frequency computed with sources above 80 % completeness. The fraction is at most 13 %, and is on average around 7 %. The intermediate source population thus has no impact on our number counts by type.

We conclude that a genuine population of intermediate sources exist (i.e. having both a thermal dust emission component and a synchrotron component) but its contribution in number is less than typically 10 % (Fig. A.1). Notice that a free-free emission can also play a role in the spectrum flattening around 100 GHz (Peel et al., 2011).

We notice, however, that this intermediate populations lies at the faint end of the flux distribution (i.e. they usually are among the faintest sources of our sample). To investigate further if the presence of intermediate sources is linked to the level of photometric noise, we performed the classification on our whole sample (i.e. including sources at fluxes below the 80 % completeness limit). The results, shown in Fig. A.2, indicates that the higher the photometric noise the more sources are classified as intermediate.

When using the total sample (i.e. with sources fainter than the 80 % completeness cut), the fraction of intermediate sources

increases, but those sources are always at the faint end of the flux distribution: the effect of the photometric noise is thus mainly responsible for this classification. This emphasises that we should use highly-complete samples for such statistical analysis, in order not to be biased towards mis-classification.

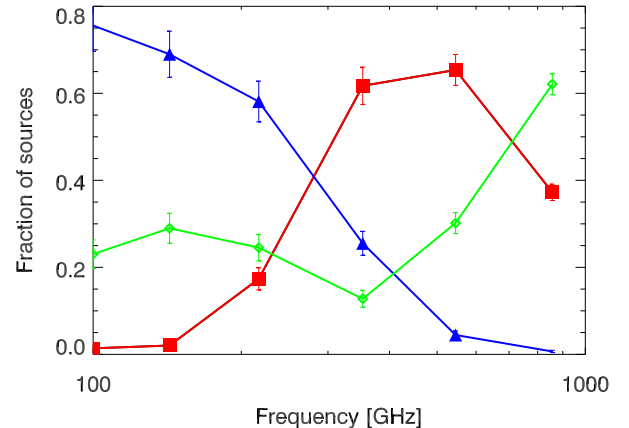


**Figure A.2.** Like Fig. A.1, the fraction of source type (dusty, red squares; synchrotron, blue triangles; green diamonds, intermediate) as a function of frequency. The difference is that we have now included the whole catalogue, i.e. including sources affected by more photometric noise below the 80 % completeness limit cut. The effect of increasing noise is to induce more sources to be classified as intermediate. This illustrates the need to cut at 80 % completeness for a robust classification.

## Appendix B: Some peculiarities, individual sources or group of sources

While the SEDs of some particular sources have been published in the *Planck* early papers Planck Collaboration XIV (2011); Planck Collaboration XV (2011); Planck Collaboration XVI (2011), we check here some specific sources detected at low or high frequency, but with unexpected classifications.

### B.1. Low-frequency dusty galaxies

There are seven low-frequency sources (three at 100 GHz and four at 143 GHz) that are classified as dusty galaxies. This kind of classification is not necessarily expected, unless we detect local galaxies showing both radio and infrared components. For this reason we check them individually.

1) PLCKERC100 G062.69–14.07: There is no radio identification in NVSS & GB6 or in NED, and no detection at LFI frequencies. This source is likely correctly classified as a dusty galaxy.

2) PLCKERC100 G140.41–17.39: This source is found with NED to be NGC 891. There is no LFI detection, but detections in NVSS/GB6. We might be seeing two components (dusty and synchrotron) of this nearby galaxy.

3) PLCKERC100 G141.42+40.57: This is NGC3034 (M82). As above we are sensitive to both components of this nearby galaxy.

4) PLCKERC143 G001.33–20.49: No LFI detection nor radio identification. This source is correctly classified as a dusty galaxy.

5) PLCKERC143 G148.59+28.70: This source is likely a blazar with an almost flat spectrum at high frequencies and detections in NVSS and GB6. This source is likely incorrectly classified as dusty, because of the small jump in flux at 545 GHz.

6) PLCKERC143 G236.47–14.38: No LFI detection nor radio identification. This source is correctly classified as a dusty galaxy.

7) PLCKERC143 G349.61–52.57: No LFI detection. At 0.2 to 20 GHz frequencies it is identified as a flat-spectrum source but its high-frequency spectrum shows a clear dusty behaviour. This source is correctly classified as a dusty galaxy, although a clear radio component is detected.

### B.2. High frequency synchrotron galaxies

There are four sources classified as synchrotron sources at 857 GHz. We also check them individually.

1) PLCKERC857 G206.80+35.82: This is a confirmed blazar detected with *WMAP*. This source is correctly classified as synchrotron-dominated.

2) PLCKERC857 G237.75–48.48: This is a confirmed blazar detected with *WMAP* and *ATCA*. This source is correctly classified as synchrotron-dominated.

3) PLCKERC857 G250.08–31.09: This is a confirmed blazar detected with *WMAP* and *ATCA*. This source is correctly classified as synchrotron-dominated.

4) PLCKERC857 G148.24+52.44: This is NGC 3408, quite faint for *Planck* at high frequencies (812 mJy at 857 GHz and not detected at 545 GHz). This source, although in our sample defined in Sect. 2.3, was not used in the number counts because of the low completeness level at this flux density.

### B.3. Bump at 4 Jy at 545 GHz in the medium zone

As discussed in Sect. 4 and shown in Fig. C.1, there is an excess of 545 GHz sources in the medium zone at 4 Jy, which is also seen at 857 GHz at 10 Jy and at 353 GHz at 1 Jy. This bump is created at 545 by 18 sources (between 3 and 5 Jy). Among the sources, we find NGC 3147, NGC 4449, NGC 4217, NGC 3992, NGC 4088, NGC 4096, NGC 4051, NGC 3631, NGC 3938, IC 0750, NGC 4244, NGC 3726, NGC 4214, NGC 7582 and NGC 7552. At 857 GHz, we find 20 sources between 7.6 and 12 Jy, with many in common. These sources are not physically associated and are spread over a large surface of the sky, although the majority lie around (150 deg., 60 deg.) in Galactic coordinates.

## Appendix C: Number counts by zone

Fig. C.1 shows the number counts for each of the three zones: deep, medium, and shallow. This illustrates the sample variance, as mentioned in Appendix B.3.

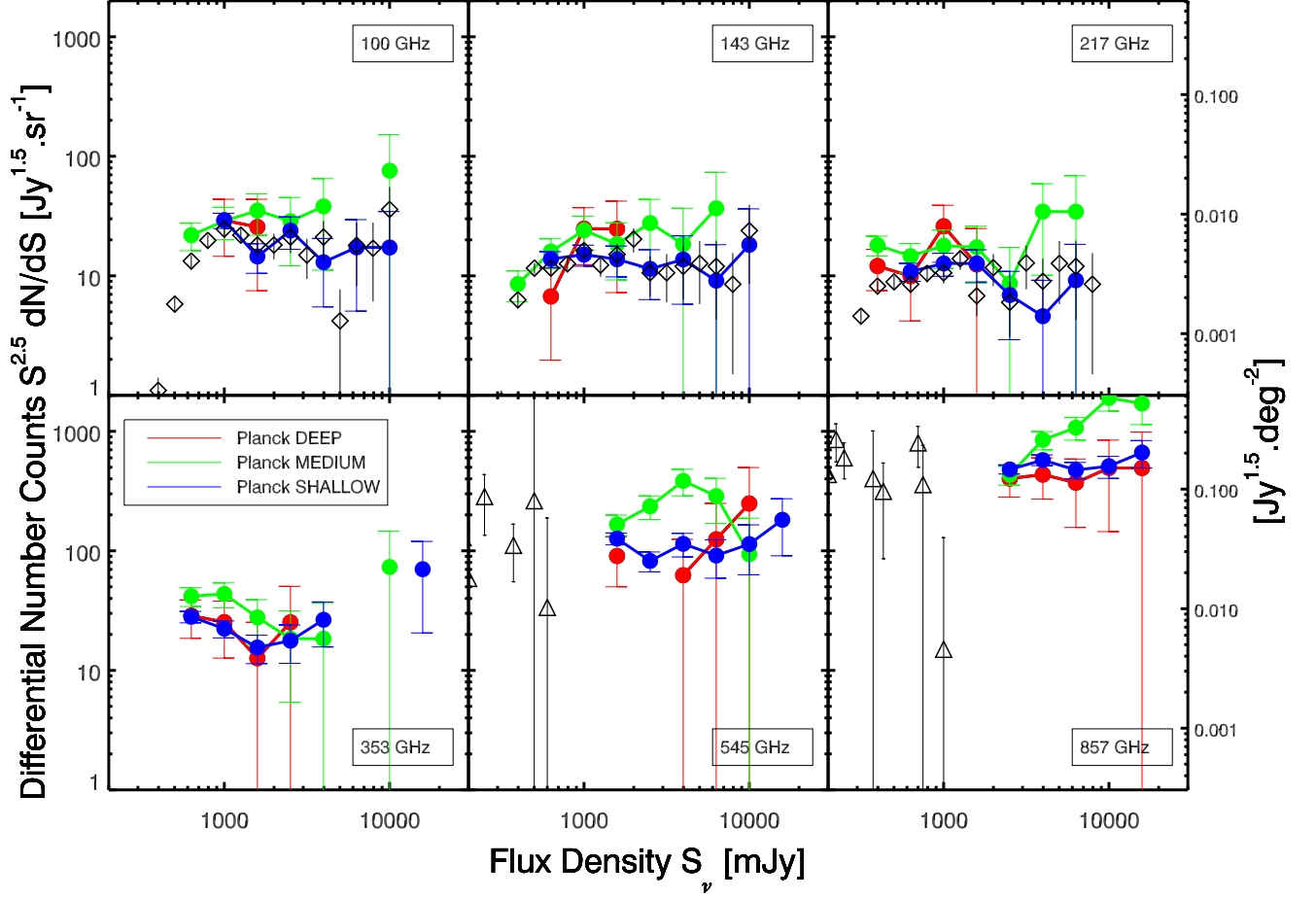


**Figure C.1.** *Planck* differential number counts (total: dusty+synch) at 6 frequencies between 100 and 857 GHz, normalized to the Euclidean, for each zone (filled circle): deep (red), medium (green) and shallow (blue). Diamonds are from *Planck* HFI ([Planck Collaboration XIII, 2011](#)), triangles from Herschel SPIRE ([Oliver et al., 2010](#); [Clements et al., 2010](#)) and BLAST [Bethérmin et al. \(2010b\)](#). The bump at 4 Jy at 545 GHz (and at 10 Jy at 857 GHz) in the medium zone is discussed in Sect. B.3.